Biogeosciences Discuss., 6, 4305–4359, 2009
www.biogeosciences-discuss.net/6/4305/2009/

Biogeosciences Discussions

Biogeosciences Discussions is the access reviewed discussion forum of *Biogeosciences*

Impact of dust deposition on Fe biogeochemistry at the Tropical Eastern North Atlantic Time-series Observatory site

Y. Ye, C. Völker, and D. A. Wolf-Gladrow

Alfred Wegener Institute for Polar and Marine Research, Bremerhaven, Germany

Received: 27 February 2009 – Accepted: 23 March 2009 – Published: 17 April 2009

Correspondence to: Y. Ye (ying.ye@awi.de)

Published by Copernicus Publications on behalf of the European Geosciences Union.

Abstract

A one-dimensional model of iron speciation and biogeochemistry, coupled with the General Ocean Turbulence Model (GOTM) and a NPZD-type ecosystem model, is applied for the Tropical Eastern North Atlantic Time-series Observatory (TENATSO) site. Aimed at investigating the role of organic complexation and dust particles in Fe speciation and bioavailability, the model is extended in this study by a more complex description of the origin and fate of organic ligands and of particle aggregation and sinking.

Model results show that the profile of dissolved iron is strongly influenced by the abundance of organic ligands. Modelled processes controlling the source and fate of ligands can well explain the abundance of strong ligands. However, a restoring of total weak ligands towards a constant value is required for reproducing the observed nutrient-like profile of weak ligands, indicating that decay time of weak ligands might be too long for a 1d-model.

High dust deposition brings not only considerable input of iron into surface waters but also fine inorganic particles for particle aggregation and Fe scavenging. Simulated profiles of dissolved iron show high sensitivity to re-dissolution of colloidal and particulate iron. The colloidal to soluble iron ratio is underestimated assuming that colloidal iron is mainly composed of inorganic colloids. That strongly argues for introducing organic colloids into the model in future work.

1 Introduction

Iron is an essential micro-nutrient for marine organisms. Its low availability in the upper ocean has been made responsible for the high-nitrate low-chlorophyll (HNLC) conditions in the Southern Ocean, the equatorial Pacific and the subpolar North Pacific (Martin and Fitzwater, 1988; Martin et al., 1990, 1994; Boyd and Abraham, 2001; Coale et al., 1996, 2004). It has been hypothesised that iron could indirectly affect primary

production in low nutrient regions by limiting nitrogen-fixation, which transforms atmospheric nitrogen into new biologically available nitrate (Mills et al., 2004.; Falkowski, 1997).

The solubility of iron is low under oxic conditions. It exists in seawater in different physical and chemical forms, e.g. inorganic soluble ferric and ferrous iron, organically complexed iron, colloidal and particulate iron. Some of these forms can be utilised by phytoplankton (Maldonado and Price, 1999; Hutchins et al., 1999) and transformed into organic particulate iron. Dissolved iron can be transported into the particulate pool also by scavenging onto particles (Balistieri et al., 1981), binding on cell surface (Hutchins et al., 2002; Tovar-Sanchez et al., 2003) and colloidal aggregation (Wells and Goldberg, 1993; Johnson et al., 1994; Wen et al., 1997). Thus, iron bioavailability is controlled by its speciation and removal from the upper water layers.

One of the most important natural sources of iron for marine systems is dust deposition. It is variable and affected by climate change (Mahowald et al., 2003; Jickells et al., 2005). How this affects marine productivity and thus the carbon cycle depends on the processes influencing iron speciation and bioavailability. Recent studies enhanced our knowledge on many reactions in Fe speciation and factors influencing them. How these individual processes interact and how ecosystems respond to varying Fe speciation, is still not well known. To provide a better understanding of this complex, several numerical models of iron cycling have been developed: global models of iron cycling primarily aimed at reproducing the scavenging removal of iron in the deep ocean (Parekh et al., 2004) or the characteristics of regions under iron limitation (Aumont et al., 2003); process-based models have been refined for coastal waters by Rose and Waite (2003a), and for the upper ocean at the Bermuda Atlantic Time-series Study (BATS) site by Weber et al. (2005, 2007). Weber et al. (2007) coupled a one-dimensional model of iron speciation and biogeochemistry with the General Ocean Turbulence Model (GOTM) and a NPZD-type ecosystem model. Our model is based on the model by Weber et al. (2007) and has been extended to include a more complex description of the origin and fate of organic ligands and of particle aggregation and

sinking. We use it to simulate the cycling of iron at the Tropical Eastern North Atlantic Time-series Observatory (TENATSO) site (17.4° N, 24.5° W), a new time-series station north of the Cape Verde Islands. The TENATSO site is strongly influenced by Saharan dust events and the mixed layer depth there has very low seasonal variability providing ideal conditions for investigation of dust deposition on Fe speciation and bioavailability. This study is focusing on two key questions: 1) the role of dust particles in Fe speciation and removal, and 2) the control of dissolved iron concentration by origin and fate of organic Fe-binding ligands.

2 Model description

Our model consists of a physical, chemical, and biological model coupled in a one-dimensional vertical water column representing the upper 400 m water depth, e.g. horizontal gradients are assumed to be small and thus neglected. The water column under consideration is divided into 67 vertical layers. Spacing increases non-linearly with depth in such a way that the uppermost layer has a thickness of 1 m and there are 28 layers in the upper 100 m. Another setup for the upper 1000 m in 100 layers has been used to compare model-generated vertical fluxes of carbon with sediment trap data. We integrated the model for a total period of 5 years, from 1 January 1990 to 31 December 1994 using the first 2 years for spin-up.

2.1 Physical model

The physical model is the General Ocean Turbulence Model (GOTM, Umlauf and Burchard, 2005, www.gotm.net), that provided the vertical mixing and advection for given forcing by wind, heat and freshwater fluxes at the surface. The model configuration is based on the configuration by Weber et al. (2007), and has been adapted for the TENATSO site by forcing the model with fluxes derived from the ECMWF atmospheric reanalysis for the TENATSO site, by choosing a slightly different turbulence parameter-

isation, and a slightly different time/space discretization.

We have used a $k-\epsilon$ turbulence closure, with a minimum turbulent kinetic energy (TKE) value of 10^{-5} m^2 s^{-2} to account for double diffusion. For time-stepping we used a modified Patankar scheme and a time-step of only 1 s, to represent fast photochemical reactions (see Sect. 2.2 Chemical model).

2.2 Chemical model

Five iron species are distinguished in the chemical part: 1) soluble (truly dissolved) inorganic ferric iron Fe(III)', which includes all hydrolysed species in the form of $Fe(OH)_n^{3-n}$; 2) soluble inorganic ferrous iron Fe(II)'; 3) organically complexed iron Fe_{lig} which is further divided into complexes with strong FeL_{str} and weak ligands FeL_{we}; 4) colloidal iron Fe_{col}; and 5) iron bound to the surface of sinking particles Fe_p. Soluble iron (Fe_{sol}) is defined here by a filter cutoff of 0.02 μm and includes Fe(III)', Fe(II)' and Fe_{lig}, colloidal iron between 0.02–0.4 μm and particulate iron >0.4 μm. The sum of the species 1)–4) represents dissolved iron (DFe) which is smaller than 0.4 μm.

The following processes converting iron between different species are included in our model (Fig. 1): 1) photo-reduction of different ferric forms: the direct photo-reduction of organically complexed iron, colloidal and particulate iron; and the indirect photo-reduction of Fe(III)' by photoreduced superoxide; 2) oxidation of Fe(II)' by oxygen, superoxide and hydrogen peroxide; 3) complex formation and dissociation; 4) scavenging of Fe(III)' onto organic and inorganic sinking particles; 5) colloid formation and re-dissolution; 6) colloidal aggregation and re-dissolution of particulate iron. Most of rate laws and constants are adopted from Weber et al. (2005) (see citation in Weber et al. (2005), Sect. 2.2). Re-dissolution of colloidal and particulate iron are shown to influence dissolved iron profile in a sensitivity study by Weber et al. (2007). The rates of these processes are still rarely reported. Here we chose the rate for colloid re-dissolution from Rose and Waite (2003b) (k_{cd}=0.41 d^{-1}) and assumed a rate for re-dissolution of particulate iron to ensure that the flux from particulate to colloidal pool is in the same order of magnitude as colloidal aggregation (k_{pd}=1.5 d^{-1}).

Weber et al. (2007) assumed a fixed concentration of free iron-binding organic ligands, in excess of DFe concentration. Sources and fate of organic ligands are still largely unknown. However, recent studies have identified a number of different marine iron-binding ligands and distinguished them by their conditional stability constants (see Sect. 4.3 Organic complexation). The vertical distribution of organic ligands are also measured in some regions (Van den Berg, 1995; Rue and Bruland, 1995; Witter and Luther III, 1998; Witter et al., 2000; Boye et al., 2001, 2006; Cullen et al., 2006; Gerringa et al., 2006, 2008.). Two types of ligands are introduced in our model: free strong ligands (L_{str}) representing marine siderophores and weak ligands (L_{we}) representing porphyrin-like ligands, as well as the different types of complexes: FeL_{str} and FeL_{we}. The concentration of free organic ligands is determined by their sources and sinks, namely biological sources, microbial decomposition, photochemical degradation, formation and dissociation of organic complex with iron, and phytoplankton uptake (see Sect. 4.3 Organic complexation). Parameterisation and estimation of the rates and constants are explained in detail in Sect. 4.3.

Another extension to Weber et al. (2007) is the classification of sinking particles. Weber et al. (2007) distinguished organic (detritus) and inorganic (deposited terrigenous material) particles only and for the sake of simplicity assumed an equal sinking rate for both. Particles in our model are split into four classes by their composition and size: 1) small detritus; 2) fine terrigenous material deposited by Saharan dust events; 3) large, pure organic aggregates and organic material in mixed aggregates; and 4) terrigenous material in mixed aggregates. This classification is based on the size distribution of sinking particles at the TENATSO site (see Sect. 4.4 Removal of dissolved iron). Two different settling velocities are assumed for the small organic and inorganic particles 1) and 2), and the aggregates 3) + 4), respectively. Particle aggregation is described as coagulation between small particles. Parameterisation and choosing of the rates and constants are explained in detail in Sect. 4.4.

Dust deposition fluxes simulated by Mahowald et al. (2003) are used for prescribing the surface flux of dust particles. The surface flux of iron is calculated with a constant

content (3.5%) of iron similar to continental crust (Wedepohl, 1995; Duce and Tindale, 1991) and 1% solubility (Johansen et al., 2000; Spokes and Jickells, 1996; Baker et al., 2006a,b). Profiles of free organic ligands in Rue and Bruland (1995) are used as initial data for ligand concentration.

2.3 Biological model

The biological part of our model is a nitrogen-based ecosystem model developed originally by Schartau and Oschlies (2003a,b). Its four compartments are nitrogen (N), phytoplankton (P), zooplankton (Z), and detritus (D). The processes and fluxes between them are mostly described in the same way as in Weber et al. (2007). In her model, the coupling between the ecosystem model and chemical model is mediated by: 1) iron uptake by phytoplankton, 2) iron release during remineralisation, 3) scavenging of iron by detritus, and 4) the influence of phytoplankton on photochemical reactions through its influence on the attenuation of light. Our model contains additional interactions between biology and iron chemistry: 1) the bioavailability of iron controls the active production of ligands, and 2) the organic complexation of iron is further affected by the release of ligands during remineralisation, and the biological and photochemical degradation of ligands; 3) furthermore, the formation of aggregates, and by that the vertical flux of adsorbed iron, is influenced by the amount of particulate organic matter.

As in Weber et al. (2007), the uptake of iron by phytoplankton follows a Michaelis-Menten dependence on the concentration of organically complexed dissolved iron, assuming that the latter is bioavailable (Maldonado and Price, 1999). The growth limitation of phytoplankton by iron is then calculated from its internal Fe:N-quota Q_{Fe} according to

$$f_{\mathrm{Fe}} = \frac{Q_{\mathrm{Fe}} - Q_{\mathrm{Fe}}^{\mathrm{min}}}{Q_{\mathrm{Fe}}} \tag{1}$$

where $Q_{\mathrm{Fe}}^{\mathrm{min}}$ is a minimal cellular Fe quota. The actual growth rate is then calculated as

the product of a light- and temperature dependent maximal growth rate with the smaller of f_{Fe} and a Michaelis-Menten-term in dissolved inorganic nitrogen.

3 Results from the physical and biological model

3.1 Physical conditions

The annual cycle of the mixed layer depth in the model is primarily driven by seasonal changes in surface heat flux and wind stress. Due to the subtropical climate, averaged daily high temperatures at the TENATSO site range only from 25°C to 29°C. The modelled thermal stratification is strong during the whole year and the mixed layer depth shows relatively low seasonal variability. The annual pattern of mixed layer depth is similar to the estimate by De Boyer Montegut et al. (2004) (Fig. 2). A characteristic feature at the TENATSO site is the existence of a shallow layer of high-salinity water underneath the winter maximum mixed layer depth, which originates from near the centre of the subtropical gyre at 30° N. Maintaining the effect of this high-salinity water on density stratification in a one-dimensional model requires an unphysical restoring term for salinity and temperature towards observations. We have used a weak uniform restoring with a time-scale of three months. Not surprisingly therefore, modelled temperature and salinity are in good agreement with observations. This restoring is weak enough to allow for a realistic high-frequency variability in mixed-layer depth.

3.2 Primary production and export

The modelled chlorophyll a concentration in surface waters is between 0.2 to 0.45 $\mu g\,L^{-1}$ and consistent with the observations at the TENATSO site or during cruises past the Cape Verde Islands, which vary from 0.06 to 0.7 $\mu g\,L^{-1}$ (Cruise data of POS 320/1, POS 332, Meteor 68/3, POS 348/2, Merian, 20 April 2008, L. Cotrim da Cunha, personal communication). Between March and November, a deep chlorophyll maximum with values around 0.4 $\mu g\,L^{-1}$ develops at the depth of nutricline near 70 m.

Primary production in the model shows a strong daily, but only a weak seasonal variation, with an annual average of 660 mg C m^{-2} day^{-1}. Primary production estimated from MODIS data, using the algorithm by Behrenfeld and Falkowski (1997) averages to 470 mg C m^{-2} day^{-1} for the 1°×1° square around the TENATSO station and the period from July 2002 to December 2007.

Phytoplankton growth is limited by nitrogen rather than iron from surface to the depth of the deep chlorophyll maximum. The lowest value of the nitrogen limiting factor f_N is around 0.3 found in surface waters during phytoplankton blooms in summer and autumn.

$$f_N = \frac{N}{N + K_N} \quad (2)$$

The iron limiting factor f_{Fe} (Eq. 1) varies between 0.66 and 0.80 and the strongest limitation is immediately below the depth of the deep chlorophyll maximum. A feedback of phytoplankton to Fe limitation is provided by the production of strong organic ligands primarily at the depth of the deep chlorophyll maximum.

About 10% of the modelled primary production is exported from the base of the winter mixed layer at 70 m, but the maximum vertical flux is 130 mg C m^{-2} day^{-1} or 20% of integrated primary production and is reached at 100 m depth, indicating a significant contribution from the deep chlorophyll maximum. This export to primary production ratio is at the higher end of typical open-ocean values which range from 5 to 25% (De La Rocha and Passow, 2007). In our model it is at least partially due to the formation of more rapidly sinking aggregates caused by the aggregation of small detritus with abundant dust particles. The average flux of organic carbon to 1000 m depth is about 50 mg C m^{-2} day^{-1}, or 38% of the flux in 100 m depth. The ratio between the fluxes at 1000 and 100 m is higher than the expected 15% from the empirical depth dependency of organic carbon flux $F(z)$ according to Martin et al. (1987)

$$F(z) = \left(\frac{z}{100\,m}\right)^{-0.8} F(z = 100\,m) \quad (3)$$

Both, the high export/production ratio and the high ratio between the fluxes at 1000 and 100 m depth may help to explain the discrepancy to regional sediment trap estimates of the flux at 1000 m depth: organic carbon flux at a mooring to the south of Cape Verde is between 2.0 and 12.7 mg C m^{-2} day^{-1} (Fischer and Wefer, 2000) and for North-west African upwelling between 3.5 and 9.3 mg C m^{-2} day^{-1} (Lutz et al., 2002). This discrepancy may point to deficiencies in our parameterisation of vertical sinking which resolves only two particle classes and that does not take into account disaggregation of particles and the variation of sinking speed with the mineral load. Minerals add density to aggregates but also decrease their size and fragment them into smaller particles if reaching a certain concentration (Hamm, 2002; Passow and De la Rocha, 2006). While the concentrations of particles in the experiments by Hamm (2002), Passow and De la Rocha (2006) were clearly higher than expected in an open-ocean region, they were performed at similar ratios of inorganic/organic particles as we find in our simulations. However, the discrepancy might also be partly due to spatial variations or to the trapping efficiency of sediment traps. As sediment trap data directly from the TENATSO site becomes available a validation of this aspect of the model and a better judgement of model deficiencies will become possible.

4 Results from the chemical model and discussions

4.1 Modelled concentration and profile of dissolved iron

Most measured profiles of dissolved iron (DFe) show a nutrient-like distribution: the minimal concentration is in surface waters and averages globally 0.07 nmol L^{-1}; like for other remineralised nutrients (Broecker and Peng, 1982), DFe concentrations increase with depth. However, unlike other nutrients, deep-water DFe show no obvious enrichment with increasing water-mass age. Concentrations in the deep ocean are rather constant near 0.6 nmol L^{-1} away from the influence of continental shelves, with lower values in the Southern Ocean and higher values in the tropical Atlantic (Johnson et al.,

1997; Wu and Boyle, 2002; Boye et al., 2006; Sarthou et al., 2007).

The modelled DFe concentration ranges in the same order as observations (Fig. 3). Due to the episodic dust deposition, the surface concentration of DFe varies from 0.28 to 0.69 nmol L^{-1} and its annual average is ca. 0.35 nmol L^{-1} which is close to the measured DFe concentration for the Cape Verde site or the region close to (Sarthou et al. (2003): 0.28 nmol L^{-1}, Sarthou et al. (2007): 0.37–0.52 nmol L^{-1}, Rijkenberg et al. (2008): 0.1–0.4 nmol L^{-1}). The DFe maximum is found in the averaged profile between 60 and 80 m due to the strongest releasing of Fe_{lig} from detritus. Below its maximum, DFe decreases strongly with depth down to ca. 150 m and then keeps its concentration constant between 0.17 and 0.2 nmol L^{-1}. Possible causes for the lower than observed concentrations of DFe in the depth are discussed in Sect. 4.4.2.

4.2 Diurnal variation of Fe speciation

The modelled Fe speciation shows a strong diurnal variability because of photochemical reactions (Figs. 4 and 5). O_2^- and H_2O_2 strongly influence the redox state of Fe. O_2^- is mainly produced by the photo-oxidation of coloured dissolved organic matter (CDOM) and the production rate in our model is proportional to light intensity. Thus the concentration of O_2^- increases after sunrise, reaches its maximum at noon and then falls to zero after sunset. H_2O_2 has a longer lifetime than O_2^-, especially in the absence of Fe(II)', and does not vanish during the night. Its rate of production which is proportional to [Fe(II)'][O_2^-] has a strong maximum at noon and rapidly decreases afterwards. Its rate of consumption, which is proportional to [Fe(II)'][H_2O_2] has a lower but broader maximum. In consequence, the concentration of H_2O_2 reaches its maximum 3–4 h after noon, when the loss becomes larger than the production.

Photo-reduction of Fe(III)' mediated by O_2^- presents a most important source of Fe(II)' in the model and its rate is more than 100 times the rate of all the direct photo-reductions together. The concentration of Fe(II)' is mainly controlled by photo-reduction mediated by O_2^- and oxidation by H_2O_2 and O_2^-. With the sunrise, Fe(II)' increases

quickly with increasing light intensity and O_2^- concentration. Photo-reduction of ferric iron overwhelms the oxidation till shortly after noon. In the afternoon, H_2O_2 reaches its maximum and light intensity becomes lower. The balance between photo-reduction and oxidation is shifted, leading to a rapid decrease of Fe(II)'. During the night, the concentration of Fe(II)' is close to 0 because of its extremely short lifetime.

Concentration of Fe(III)' is mainly controlled by Fe(II)' oxidation and organic complexation. During the day, Fe(III)' has a low concentration and shows a rapid increase after sunset. However, organic complexation leads to a decrease of Fe(III)' after 08:00 pm again, such that Fe_{lig} (both FeL_{str} and FeL_{we}) are the dominant forms during the night in summer and throughout the daily cycle in winter.

Fe_{col} shows a lower sensibility to changes in light than Fe_{lig}, since colloid formation is a much slower process than oxidation and organic complexation (Rose and Waite, 2003a).

The pattern of the daily cycle in winter is similar to that in summer, but shows a smaller amplitude caused by the weaker irradiance and deeper mixed layers in winter. Fe_{lig} has a much higher concentration than in summer. One of the reasons is the decrease of photoredox reaction rate, and another one that dust deposition at the TENATSO site is mostly more intensive in winter than in summer which results in a higher iron input in winter.

Weber et al. (2005) demonstrated the influence of copper on the amplitude of the daily cycle of superoxide concentration and Fe speciation. We considered the role of copper in the same way like Weber et al. (2005). In our model, increasing Cu concentration from 1 nmol L^{-1} to 5 nmol L^{-1} reduces the daily amplitude of Fe(II)' to a third of its value. We estimated Cu concentration according to the measurements by Van Der Loeff et al. (1997) showing a varying range of Cu between 0.5 to 1.3 nmol L^{-1} near Cape Verde Islands. Because Fe redox speciation has not yet been measured at the TENATSO site, we compared the modelled H_2O_2 with observations. By choosing a total concentration of copper of 1 nmol L^{-1}, the modelled H_2O_2 integrated for 0–200 m ranges from 3 to 7 mmol m^{-2} which is comparable with a H_2O_2 inventory of about

3.7 mmol m^{-2} for the same depth interval measured in the vicinity (Steigenberger and Croot, 2008).

4.3 Organic complexation

Existence and concentration of organic ligands in seawater affect Fe speciation considerably. 99% of dissolved Fe is organically complexed (Gledhill and van den Berg, 1994; Van den Berg, 1995; Rue and Bruland, 1995; Wu and Luther III, 1995; Witter and Luther III, 1998). Most measurements of iron organic complexation show an excess of free ligands over dissolved iron and relatively constant concentration of ligands in deep waters (Rue and Bruland, 1995; Van den Berg, 1995; Wu and Luther III, 1995; Boye et al., 2001, 2006; Gerringa et al., 2006, 2008.).

Identity, origin and chemical characteristics of organic ligands are widely unknown. Nevertheless, two classes of organic ligands distinguished by their conditional stability constants ($K_{Fe'L}$) are often determined in field studies: a strong ligand class with log $K_{Fe'L}$ ranging from 12 to 13 and a weak one with log $K_{Fe'L}$≈11 (Rue and Bruland, 1995, 1997; Wu and Luther III, 1995; Macrellis et al., 2001). Rue and Bruland (1995) showed that strong ligands decrease rapidly with depth below the surface maximum, whereas the concentration of weak ligands increases with depth and doubles at 500 m.

What controls the distribution of these ligands in the water column? Sources and sinks of organic ligands are reported to be tightly connected to biological activities. Some marine microorganisms, mostly heterotrophic bacteria and cyanobacteria, produce siderophores to facilitate Fe uptake (Trick, 1989; Reid et al., 1993; Wilhelm and Trick, 1994; Wilhelm et al., 1996; Granger and Price, 1999; Martinez et al., 2000; Martinez and Haygood, 2001; Martinez et al., 2003; Barbeau et al., 2001; Macrellis et al., 2001). This siderophore production is widely supposed to be regulated by iron level (Reid et al., 1993; Wilhelm and Trick, 1994; Wilhelm et al., 1996; Macrellis et al., 2001). However, increase of ligands was observed after iron fertilisation indicating that some marine organisms release ligands only to keep iron in solution as much as pos-

sible (Rue and Bruland, 1997; Bowie et al., 2001). The conditional stability constant of siderophores is similar to that of the naturally occurring strong ligands in seawater (Rue and Bruland, 1995; Lewis et al., 1995; Macrellis et al., 2001).

Porphyrin-type ligands can be released by cell lysis (Poorvin et al., 2004; Gerringa et al., 2006) and zooplankton grazing (Sato et al., 2007; Kondo et al., 2008), and is supposed to be released as degradation products of cytochrome system (Boye et al., 2001). The conditional stability constant of porphyrins is within the range of the weak ligand class in seawater (Rue and Bruland, 1995, 1997; Witter et al., 2000; Luther et al., 2001; Macrellis et al., 2001). This provides the basis for our assumption of source of weak ligands.

Organic ligands are often photochemically reactive (Johnson et al., 1994; Barbeau et al., 2001, 2003; Powell and Wilson-Finelli, 2003; Maldonado et al., 2005; Rijkenberg et al., 2006, 2008). Some studies show that the product of photolysis of strong ligands retains the ability to complex Fe(III)' (Barbeau et al., 2001, 2003; Powell and Wilson-Finelli, 2003). Other sinks of organic ligands are biological uptake (Powell and Wilson-Finelli, 2003; Hutchins et al., 1999; Maldonado and Price, 1999; Wang and Dei, 2001), bacterial decomposition of free ligands (Kondo et al., 2008) and adsorption onto particles (Powell and Wilson-Finelli, 2003).

Based on these studies on organic iron binding ligands, we tried to explain observed ligand distribution and corresponding changes in Fe speciation by modelling the sources and sinks of organic ligands (Fig. 6). There are two classes of organic ligands in the model representing strong (L_{str}) and weak ligands (L_{we}). Processes controlling concentration of these ligands are: active ligand production by phytoplankton, release of ligands during remineralisation, organic complexation with Fe(III)' and complex dissociation, uptake by phytoplankton, photochemical and biological degradation of ligands.

In the model, strong ligands are produced by phytoplankton (P) under Fe-limitation, where cell nitrogen is transformed into the ligand pool. To keep the simplicity of the biological model, we did not distinguish prokaryotic and eukaryotic phytoplankton and

tuned the rate of ligand production so that a reasonal phytoplankton growth can be retained by the given concentration of organically complexed iron. The ligand production rate is regulated by the internal Fe:N-quota of phytoplankton (Eq. A13). Weak ligands are released during remineralisation of detritus (D) and by photo-reactions of the strong Fe-ligand complex (FeL_{str}). The release rate of weak ligands from detritus is proportional to the detritus abundance times its remineralisation rate. The rate of ligand release varies by different organisms and is still largely unknown. In our model, we tuned the rate so that reasonable phytoplankton growth can be supported by sufficient complexed iron.

Organic complexes with both strong and weak ligands are degraded by photolysis. We assumed that the oxidised ligands released by photolysis of FeL_{str} retain a lower ability to form organic complexes with Fe(III)' and function as weak ligands, and the ligands oxidised by photolysis of FeL_{we} lose their binding ability completely. Fe_{lig} photoreduction rates (K_{phls} and K_{phlw}, Table 3) are taken from the experimental data by Rose and Waite (2003c) and were adapted to the light condition in our model. Both strong and weak ligands are remineralised by microorganisms at the same rate as remineralisation of dissolved organic matter (DOM) (Martinez et al., 2000; Amon and Benner, 1994). Phytoplankton take up all the forms of complexed iron at the same rate.

Our modelled concentration of total strong ligands (Fig. 7) is close to the measured data by Rue and Bruland (1995). Strong ligands reach their maximum ($0.57\,nmol\,L^{-1}$) at the depth of subsurface chlorophyll maximum (80 m). That indicates that phytoplankton grow in surface waters under Fe-limitation and their growth is supported by releasing organic ligands into seawater. The major sink of strong ligands near surface is the photochemical degradation of FeL_{str} with a maximal rate of ca. $2.9\times10^{-3}\,d^{-1}$. Deeper in the water column, biological degradation of free ligands dominates. The maximal rate of biological degradation is $3.4\times10^{-2}\,d^{-1}$ between 70 and 80 m. Below 80 m, strong ligands decline rapidly with depth.

Looking at the modelled profile of total weak ligands, two points are noticeable: 1) Weak ligands increase continuously from surface to the depth of detritus maximum

which is in agreement with the observations. The absolute concentration of weak ligands is higher than that of strong ligands; 2) Contrary to the observations, modelled weak ligands decrease exponentially with depth below its maximum at 90 m and reach a relatively low concentration below 300 m (≈0.4 nmol L^{-1}).

Several factors could lead to this difference compared to observed profiles. First of all, bacterial activity is more strongly controlled by temperature compared to phytoplankton (Reinthaler et al., 2006; Pomeroy and Wiebe, 2001). In our model, the rate of remineralisation depends directly on temperature. We applied the same temperature dependence for phytoplankton growth and for remineralisation, which could lead to overestimating bacterial activity in deeper, colder waters and thus the loss rate of organic ligands. To test this, we changed the factor by which remineralisation decreases with a 10 degree temperature decrease (Q10) from 2 to 3 while keeping the remineralisation rate at 20°C constant (Eq. A7). Because the isothermal curve of 20°C ranges between 75 and 85 m during a year, the profile of total weak ligands shows different responses above and below 80 m (Fig. 8): in the upper 80 m, remineralisation is strengthened with temperature increasing above 20°C and concentration of total weak ligands is lower than in the previous model run; below 80 m, there are more weak ligands, because remineralzation rate decreases faster with temperature; a higher maximum of weak ligands is found at larger depth (ca. 100 m), because detritus is also remineralised more slowly below 80 m and thus more detritus sinks down and releases weak ligands there. However, the ligand concentration still decreases with depth below the remineralisation maximum in this model setup, in contrast to almost constant concentrations in observations.

A possible explanation the difference between our model result and the observations is that the weak ligands contain a significant fraction of refractory material that is degraded more slowly than we have assumed. In consequence we would probably have overestimated the fraction of ligands released during the remineralisation of sinking organic matter. If this is the case, then weak ligands would accumulate and ocean circulation and mixing would lead to a more homogeneous distribution in the deep ocean

(Kondo et al., 2008). Such a scenario, however, cannot be described adaequately by a one-dimensional model which only takes into account local processes. For further sensitivity studies of our model we have therefore introduced a restoring of the concentration of total weak ligands towards 2 nmol L^{-1}, a commonly observed value in the deep ocean, throughout the water column with a rate of 0.1 d^{-1}, in order not to affect iron speciation and losses by too little complexation. This restoring is weak enough so that loss processes near the surface (biological uptake and photochemical decay) still lead to the observed vertical gradient of total weak ligand concentration there.

4.4 Removal of dissolved iron

Removal processes of dissolved Fe control its residence time and thus bioavailability. In our model there are three major removal processes: biological uptake of Fe_{lig}, Fe(III)' scavenging and aggregation of Fe_{col}. We studied the role of particle size and aggregation in removing dissolved iron, and carried out sensitivity studies to examine the impact of re-dissolution of colloidal and particulate iron on controlling the vertical distribution of iron.

4.4.1 Particle size and settling

Settling velocity of particles depends directly on their size, density and porosity. Aggregation, disaggregation, degradation of organic matter, fragmentation, mineral scavenging and other processes change the character of sinking particles and thus their settling velocities (Honjo et al., 1982; Armstrong et al., 2002; Francois et al., 2002; Hamm, 2002; Klaas and Archer, 2002; Passow, 2004; Passow and De la Rocha, 2006; De La Rocha and Passow, 2007). The impact of mineral on organic particles has been proposed in the "ballast hypothesis" that biogenic and lithogenic minerals protect the organic matter from oxidation or increase the sinking velocity (Armstrong et al., 2002; Francois et al., 2002; Klaas and Archer, 2002). Another view to the relationship between mineral and biological particles is that the sinking particles control the mineral

flux by scavenging suspended minerals which are too small to sink on their own (Balistieri et al., 1981; Honjo et al., 1982; Wen et al., 1997; Passow, 2004). Therefore, studying the influence of sinking particles on Fe flux requires examination of the particle distribution in different size classes.

Fine particles dominate in Saharan dust (Guieu et al., 2002; Heinold et al., 2007). Modelled dust deposition (Heinold et al., 2007) at the TENATSO site shows that over 80% of the dust deposition is to find with particle radius varying between 0.3 and 2.6 μm in a typical month with high deposition. Therefore, particles in our model are distinguished into two size classes: a small one which has a mean size of 10 μm and consist of single phytoplankton cells, small detritus (D) and dust particles (B), and a large one representing aggregates which has a mean size of 100 μm and is divided into an organic (A_{or}) and inorganic (A_{in}) fraction. We assigned two different sinking velocities for the size classes, respectively: the small particles sink at 5 m d^{-1} (except for phytoplankton cells which do not sink), and the large ones sink at 50 m d^{-1} (Smayda, 1970; Asper et al., 1992; Asper and Smith, 2003; Kriest, 2002).

Particle aggregation increases the removal rate of small suspended particles by transforming them into large, rapidly settling particles (McCave, 1984; Jackson and Burd, 1998). Burd and Jackson (2009) explored different coagulation mechanisms and expressions for coagulation kernels as functions of particle radius. We compared the relative importance of each mechanism for within and between the two size classes of particles in the model (Table 1). Small particles coagulate mainly by Brownian motion and turbulent shear, whereas differential sedimentation dominates the coagulation between small and large particles. Saharan dust deposition leads to very high abundance of fine particles in seawater in the modelling region, thus we described particle aggregation only as coagulation between small particles. The aggregation rate depends on the concentration of all the small particles: phytoplankton, detritus and dust particles. Biomass of phytoplankton and detritus contributing to aggregation flows to the organic pool of aggregates and mass of dust particles flows to the inorganic pool of aggregates (Eq. A9). The maximal coagulation rate is taken from Gruber et al. (2006). It is notice-

able that turbulent shear is an important process for both size combinations and thus a dependence of coagulation rate on turbulence kinetic energy might be introduced in future work.

The modelled vertical particle distribution shows a high abundance of small particles in surface waters which decreases rapidly with depth (Fig. 9). Concentration of aggregates is low at the surface and increases with depth. Below 200 m, the concentration of aggregates is in excess of that of small particles. The averaged particle size rises with depth. Inorganic particles dominate the particle distribution throughout the water column (Fig. 10). Based on this vertical distribution of particles, scavenging of dissolved iron is dominated by adsorption onto small inorganic particles near the surface and onto aggregates deeper in the water column.

This distribution pattern can be explained by: 1) Saharan dust events massively bring massive small particles into seawater resulting in high concentration of fine inorganic particles throughout the water column; 2) particle aggregation changes the small to large particles ratio. The concentration increase of aggregates with depth is more slowly than the concentration decrease of small particles, because a considerable part of aggregates is removed by more rapidly sinking.

However, the modelled transport from small to large particles depends on the total concentration of small particles and proportional to the relative abundance of each class of small particles. That results in a similarity between the composition of aggregates (A_{in}:A_{or}) and the small inorganic to organic particle ratio (B:D). Because dust particles mostly dominate the particle distribution at the TENATSO site, the composition of aggregates could be unrealistic. To test this hypothesis, we compared the modelled A_{in}:A_{or} ratio with the saturating capacity of organic aggregates for mineral particles from the literature and found out, that over 80% of our result exceeds the 97 to 98 weight-percent (Passow and De la Rocha, 2006). This argues strongly for introducing a dependence of aggregation on the organic fraction of aggregates into the description of particle aggregation in the model.

4.4.2 Role of particles in removing dissolved iron

Abundance and dynamics of particles control the vertical transport and residence time of iron by direct scavenging Fe' and aggregation of colloidal iron. In both cases, suspended, dissolved iron adsorbs onto particle surface and is removed in particulate form (Balistieri et al., 1981; Nyffeler et al., 1984; Johnson et al., 1997; Wells and Goldberg, 1993; Wen et al., 1997). In our model both small and large particles scavenge Fe(III)' and determine the aggregation rate of Fe_{col} (Fig. 11, Eq. A15–A22). There is no backward reaction for scavenging and the model sensitivity to the pathway from particulate back to colloidal iron is analysed below.

Without a pathway from Fe_p to DFe (Fig. 15, solid line), DFe concentration decreases continuously below its maximum at 50 m and nearly vanishes at 300 m. This disagrees with measured DFe profiles. In this model design, the rate of DFe decrease in deeper waters is mainly determined by the rate of Fe(III)' scavenging and colloidal aggregation minus the rate of biological release of FeL_{we}. Thus, the strong decrease of DFe is caused by the decreasing rate of FeL_{we} release with depth due to its dependence on detritus abundance and temperature.

Comparing the fluxes between Fe species (Fig. 12), colloid aggregation represents in both surface and deeper waters the most important loss of DFe. Biological uptake is the second important loss of DFe in surface waters and negligible in deeper waters. Scavenging of Fe(III)' also shows a higher rate in surface than deeper waters, however, it is 2 orders of magnitude smaller than that of colloidal aggregation. Therefore, the pathway from colloid formation via colloidal aggregation to sedimentation plays the key role in removing DFe.

To reduce the loss of DFe in deeper waters, we introduced re-dissolution of colloidal and particulate iron into the model. The mechanisms of these processes are still not well understood (Moffet, 2001). The vertical distributions of particulate and dissolved Th, another particle-reactive element, seem to require a desorptive pathway to explain continuous increases in depth of both Th fractions (Bacon and Anderson, 1982). The

experiments on Th by Moore and Hunter (1985) support strongly that the adsorption of Th by marine suspended particles is a reversible process. Other model results (Parekh et al., 2004; Weber et al., 2007) also show that it is necessary to introduce a pathway from particulate to dissolved iron in order to reproduce the constant non-vanishing concentration of DFe in deep-water. We studied the impact of these backward processes on the distribution of DFe in two sensitivity studies: 1) only re-dissolution of Fe_{col} is introduced; and 2) re-dissolution of both Fe_{col} and Fe_p is introduced.

In the first sensitivity study, no obvious effect is found on total DFe concentration in deeper waters (Fig. 15, dash-dot line). Assuming that all the reactions are in steady-state (Fig. 13), the total concentration of DFe is determined by the flux of colloidal aggregation and release of Fe_{lig} during remineralisation. Colloid re-dissolution directly adds a flux from Fe_{col} to Fe(III)' and thus increases the fraction of Fe(III)' and Fe_{lig} within the total DFe because organic complexation and complex dissociation are much faster reactions than all others at this depth. Hence, the Fe_{col}:Fe_{sol} (soluble iron including Fe(III)', Fe(II)' and Fe_{lig}) ratio in the deeper waters falls dramatically down to 1:200 compared to 1:67 in the model run without colloid re-dissolution, but the total amount of them does not change much.

In the second sensitivity study, introducing re-dissolution of both colloidal and particulate iron (Fig. 14) leads to a much higher concentration of total DFe. Its decline with depth becomes more gradual (Fig. 15, dashed line) because a part of Fe_p is transformed back into the dissolved pool and prevented from sinking. The total amount of dissolved iron is determined here by sinking flux of particulate iron and Fe_{lig} release. The Fe_{col}:Fe_{sol} ratio in deeper waters rises to 1:125 which is still too low compared to the observed ratios which are close to 1:1 (Wu et al., 2001; Cullen et al., 2006; Bergquist et al., 2007).

To obtain a more realistic Fe_{col}:Fe_{sol} ratio, we conducted a further sensitivity study by reducing the rate of colloid re-dissolution. The Fe_{col}:Fe_{sol} ratio rises to 1:25 and the concentration of DFe becomes constant below 180 m (Fig. 15, dotted line). However, the total DFe concentration is apparently lower than observations. Furthermore, the

Fe_{col}:Fe_{sol} ratio is still far away from the observations. Fe_{col} in the model represents only the inorganic colloidal iron which is formed by Fe(III)' and removed from the dissolved pool by colloidal aggregation. The observed, relatively constant ratio of Fe_{col} and Fe_{sol} in deep-water indicates that a fraction of colloidal iron must be prevented from removing processes (Wu et al., 2001; Cullen et al., 2006; Bergquist et al., 2007). One possible explanation could be the co-existence of organic colloids. Organic complexes of iron are found in both soluble and colloidal form (Wu et al., 2001; Cullen et al., 2006). It is reported that remineralisation releases Fe_{lig} preferentially in colloidal form (Bergquist et al., 2007). We suggest that organic colloids could be kept longer in the dissolved pool and be more biologically available than the inorganic colloids by transformation into soluble organic complexes via ligand exchange reactions. Hence, introducing organic colloidal iron in further modelling works may be helpful for reproducing the observed Fe_{col}:Fe_{sol} ratio in deep waters.

5 Summary and conclusions

A one-dimensional model of iron biogeochemistry developed for the BATS site (Weber et al., 2007) has been extended for the TENATSO site with a more complex description of origin and fate of organic ligands and particle aggregation and sinking.

Despite the simplicity of the NPZD-type ecosystem model, observed chlorophyll a concentration and seasonality of primary production at the TENATSO site are well reproduced. Averaged primary production is a little higher than satellite-derived estimates. Export production is in agreement with published values. Apart from the effect of overestimated primary production, export at 1000 m depth is still higher than estimates based on sediment trap data, indicating that the model description of particle aggregation and sinking still needs to be improved.

Sources and decay of organic ligands are connected to biological activities. The profile of dissolved iron is strongly influenced by abundance of organic ligands. Modelled processes controlling concentration of ligands can well explain the abundance of

strong ligands. However, a restoring of total weak ligands towards a constant value is required for reproducing the observed nutrient-like profile of weak ligands. This possibly indicates that weak ligands contain a fraction of more refractory material than we have assumed, and that the dynamics of this refractory material cannot be described well with a one-dimensional model. Processes affecting production and decay of these ligands need to be studied further.

High dust deposition at the TENATSO site brings, on the one hand, considerable input of iron into surface waters, and on the other hand, provides inorganic particles for Fe scavenging and particle aggregation accelerating the removal of dissolved iron. This double role of dust deposition should be taken into account in investigating the impact of varying dust deposition on Fe speciation and biogeochemistry.

Re-dissolution of colloidal and particulate iron plays an important role in preventing dissolved iron in deep waters from rapid removal. Changing re-dissolution rate of colloidal iron impacts the Fe_{col}:Fe_{sol} ratio, but is not sufficient to explain the observed large fraction of colloidal Fe in deep waters. Underestimation of this ratio indicates that iron complexed by organic colloidal ligands could be an important fraction of colloidal iron and should be introduced in future work.

Appendix A

Model equations

The rate of change of biogeochemical variables can be separated into a biogeochemical and a physical part:

$$\frac{\partial}{\partial t}X = BIO + M(X, z) \quad \text{(A1)}$$

where advection and mixing are taken into account in the physical part $M(X, z)$. Here M stands for the advection and mixing operator and X is the mixed compound. The biogeochemical rate of change is described by corresponding sources minus sinks.

The change of the biological variables N, P, Z and D (in μmol L^{-1}) is decribed by:

$$\frac{\partial}{\partial t}N=\gamma_d\, f_T\ (D+A_{or})+\gamma_{zb}\, f_T\, Z+p\, f_T\, P+\gamma_l\, f_T\ (L_{str}+L_{we})-\mu\, P+M(N,z) \quad \text{(A2)}$$

$$\frac{\partial}{\partial t}P=(\mu-p\, f_T)\ P-f_G\, Z-\gamma_{p^2}\, P^2-r_L\, \gamma_{lp}\, f_Q\, P+M(P,z) \quad \text{(A3)}$$

$$\frac{\partial}{\partial t}Z=\gamma_{za}\, f_G\, Z-\gamma_{zb}\, f_T\, Z-\gamma_{z^2}\, Z^2+M(Z,z) \quad \text{(A4)}$$

$$\frac{\partial}{\partial t}D=\gamma_{p^2}\, P^2+(1-\gamma_{za})\ f_G\, Z-(\gamma_d+r_L\, \gamma_{ld})\ f_T\, D-k_{coag}\, D\ (B+D\, r_{\mathrm{m:N}}+P\, r_{\mathrm{m:N}})-w_s\, \frac{\partial D}{\partial z}+M(D,z) \quad \text{(A5)}$$

where μ is the growth rate of phytoplankton regarding light, temperature and nutrient limitation. $\gamma_{lp}\, f_Q\, P$ describes the loss of nitrogen due to the excretion of iron-binding ligands and r_L is a factor converting ligand nitrogen (nmol L^{-1}) into phytoplankton and detritus nitrogen (μmol L^{-1}). The grazing function f_G depends on the maximal grazing rate g, the prey capture rate ϵ and phytoplankton concentration:

$$f_G=\frac{g\, \epsilon\, P^2}{g+\epsilon\, P^2} \quad \text{(A6)}$$

The rate of remineralisation is related to temperature by:

$$f_T=0.3\, C_2^{T(z)} \quad \text{(A7)}$$

which represents a temperature dependence for Q10=3.

Further sinking particles are dust particles B and the inorganic fraction of aggregates A_{in} (both in kg L^{-1}) and the organic fraction A_{or} (in μmol L^{-1}). Coagulation is decribed by a coagulation constant k_{coag} times the quadratic concentration of small particles minus sinking and biological decomposition:

$$\frac{\partial}{\partial t}B=F_{\mathrm{dust}}-k_{coag}\, B\ (B+D\, r_{\mathrm{m:N}}+P\, r_{\mathrm{m:N}})-w_s\, \frac{\partial B}{\partial z}+M(B,z) \quad \text{(A8)}$$

$$\frac{\partial}{\partial t}A_{in}=k_{coag}\,B\,(B+D\,r_{m:N}+P\,r_{m:N})-w_l\,\frac{\partial A_{in}}{\partial z}+M(A_{in},z) \quad \text{(A9)}$$

$$\frac{\partial}{\partial t}A_{or}=k_{coag}\,D\,(B+D\,r_{m:N}+P\,r_{m:N})+\gamma_{z^2}\,Z^2-\gamma_d\,f_T\,A_{or}-w_l\,\frac{\partial A_{or}}{\partial z}+M(A_{or},z) \quad \text{(A10)}$$

where F_{dust} is the deposition of dust at the ocean surface. The loss of zooplankton by its mortality $\gamma_{z^2}\,Z^2$ is considered as a source of organic aggregates.

Processes controlling ligand concentration are described as ligand production by phytoplankton or release during remineralisation + release of free ligands by complex dissociation – ligands complexed with Fe(III)' – biological decomposition of free ligands + the physical term. An additional source of weak ligands is photolysis of strong complexes $k_{phls}\,f_l\,FeL_{str}$.

$$\frac{\partial}{\partial t}L_{str}=\gamma_{lp}\,f_Q\,P+k_{flsd}\,FeL_{str}-k_{fel}\,Fe(III)'\,L_{str}-\gamma_l\,f_T\,L_{str}+M(L_{str},z) \quad \text{(A11)}$$

$$\frac{\partial}{\partial t}L_{we}=\gamma_{ld}\,f_T\,D+k_{flwd}\,FeL_{we}+k_{phls}\,f_l\,FeL_{str}-k_{fel}\,Fe(III)'\,L_{we}-\gamma_l\,f_T\,L_{we}+M(L_{we},z) \quad \text{(A12)}$$

where the production rate of strong ligands is regulated by the internal Fe:N-quota of phytoplankton:

$$f_Q=\frac{Q_{Fe}^{max}-Q_{Fe}}{Q_{Fe}^{max}} \quad \text{(A13)}$$

and a function of light intensity f_l is introduced in all photochemical reactions:

$$f_l=\frac{par(z)}{ir_{max}} \quad \text{(A14)}$$

where $par(z)$ is the photosynthetically active radiation in the given vertical layer z.

The description of the concentration change of different Fe forms is more complex than in Weber et al. (2007) due to our introduction of more than one type of particles and ligands. The equations are:

$$\frac{\partial}{\partial t}Fe(III)' = F_{\mathrm{Fe(III)',surf}} + \left(k_{ox1}\,O_2 + k_{ox2}\,O_2^- + k_{ox3}\,H_2O_2\right) Fe(II)' + k_{cd}\,Fe_{col} + k_{flwd}\,FeL_{we} + k_{flsd}\,FeL_{str} - \left(k_{fel}\,(L_{str}+L_{we}) + k_{ph3}\,f_l + k_{red}\,f_l\,O_2^-\right. + \left. k_{sca}\,(B + A_{in} + r_{\mathrm{m:N}}\,D + r_{\mathrm{m:N}}\,A_{or}) + k_{col}\right) Fe(III)' + M(Fe(III)', z) \quad \text{(A15)}$$

where the flux of Fe(III)' at the surface $F_{\mathrm{Fe(III)',surf}}$ is calculated from modelled dust deposition by Mahowald et al. (2003) F_{dust} with 3.5% Fe content in dust and 1% solubility.

$$\frac{\partial}{\partial t}Fe(II)' = f_l\,\left(\left(k_{red}\,O_2^- + k_{ph3}\right) Fe(III)' + k_{phls}\,FeL_{str} + k_{phlw}\,FeL_{we} + k_{ph1}\,Fe_{col}\right) + k_{ph4}\,\left(Fe_{part} + Fe_{aggr}\right) - \left(k_{ox1}\,O_2 + k_{ox2}\,O_2^- + k_{ox3}\,H_2O_2\right) Fe(II)' + M(Fe(II)', z) \quad \text{(A16)}$$

$$\frac{\partial}{\partial t}FeL_{str} = k_{fel}\,Fe(III)'\,L_{str} - k_{flsd}\,FeL_{str} - f_l\,k_{phls}\,FeL_{str} - k_{upt}\,\frac{FeL_{str}}{FeL_{str}+FeL_{we}} + M(FeL_{str}, z) \quad \text{(A17)}$$

$$\frac{\partial}{\partial t}FeL_{we} = \gamma_d\,f_T\,D_{Fe} + p\,f_T\,P_{Fe} + \gamma_z b\,f_T\,Z_{Fe} + k_{fel}\,Fe(III)'\,L_{we} - k_{flwd}\,FeL_{we} - f_l\,k_{phlw}\,FeL_{we} - k_{upt}\,\frac{FeL_{we}}{FeL_{str}+FeL_{we}} + M(FeL_{we}, z) \quad \text{(A18)}$$

The uptake rate k_{upt} of FeL_{str} and FeL_{we} by phytoplankton is determined by:

$$k_{upt}=\min\left(\mu_{\max}\frac{FeL_{str}+FeL_{we}}{(FeL_{str}+FeL_{we}+K_{\mathrm{Fe}})}P,\ \mu Q_{\mathrm{Fe}}^{ave}P\right) \tag{A19}$$

Choosing the smaller one of the terms ensures a dependence of uptake on Fe_{lig} availability and a storage uptake is not considered.

$$\begin{aligned}\frac{\partial}{\partial t}Fe_{col}=&k_{col}\,Fe(III)'+k_{pd}\,\left(Fe_{part}+Fe_{aggr}\right)\\&-k_{ag}\,(B+A_{in}+r_{\mathrm{m:N}}\,D+r_{\mathrm{m:N}}\,A_{or})\,Fe_{col}\\&-k_{cd}Fe_{col}-f_l\,k_{ph1}\,Fe_{col}+M(Fe_{col},z)\end{aligned} \tag{A20}$$

$$\begin{aligned}\frac{\partial}{\partial t}Fe_{part}=&\left(k_{sca}\,Fe(III)'+k_{ag}\,Fe_{col}\right)(B+r_{\mathrm{m:N}}\,D)\\&-\left(f_l\,k_{ph4}+k_{pd}\right)\,Fe_{part}-w_s\,\frac{\partial Fe_{part}}{\partial z}+M(Fe_{part},z)\end{aligned} \tag{A21}$$

$$\begin{aligned}\frac{\partial}{\partial t}Fe_{aggr}=&\left(k_{sca}\,Fe(III)'+k_{ag}\,Fe_{col}\right)(A_{in}+r_{\mathrm{m:N}}\,A_{or})\\&-\left(f_l\,k_{ph4}+k_{pd}\right)\,Fe_{aggr}-w_l\,\frac{\partial Fe_{aggr}}{\partial z}+M(Fe_{aggr},z)\end{aligned} \tag{A22}$$

Finally, a variable Fe:N-quota is introduced in P, Z, and D and evolution of the respective Fe concentrations P_{Fe}, Z_{Fe} and D_{Fe} is decribed by:

$$\frac{\partial}{\partial t}P_{Fe}=k_{upt}\,(FeL_{str}+FeL_{we})-Q_{\mathrm{Fe}}\left(f_G\,Z+\gamma_{p^2}\,P^2\right)-p\,f_T\,P_{Fe}+M(P_{Fe},z) \tag{A23}$$

$$\frac{\partial}{\partial t}Z_{Fe}=Q_{\mathrm{Fe}}\,\gamma_{za}\,f_G\,Z-\gamma_{zb}\,f_T\,Z_{Fe}-Q_{Z\mathrm{Fe}}\,\gamma_{z^2}\,Z^2+M(Z_{Fe},z) \tag{A24}$$

$$\frac{\partial}{\partial t} D_{Fe} = Q_{\mathrm{Fe}}\, \gamma_{p^2}\, P^2 + Q_{\mathrm{Fe}}\, (1-\gamma_{za})\, f_G\, Z$$
$$-\gamma_d\, f_T\, D_{Fe} - k_{coag}\, D_{Fe}\, (B + D\, r_{\mathrm{m:N}} + P\, r_{\mathrm{m:N}}) + M(D_{Fe}, z) \quad \text{(A25)}$$

where $Q_{Z\mathrm{Fe}}$ is the Fe:N-quota in zooplankton. The Fe included in the organic agrregates $A_{or,Fe}$ has the same sources and sinks as A_{or}:

$$\frac{\partial}{\partial t} A_{or,Fe} = k_{coag}\, D_{Fe}\, (B + D\, r_{\mathrm{m:N}} + P\, r_{\mathrm{m:N}}) + Q_{Z\mathrm{Fe}}\, \gamma_{z^2}\, Z^2$$
$$-\gamma_d\, f_T\, A_{or,Fe} - w_l\, \frac{\partial A_{or,Fe}}{\partial z} + M(A_{or,Fe}, z) \quad \text{(A26)}$$

Acknowledgements. This work is a contribution to the project SOPRAN (Surface Ocean Processes in the ANtropocene), which is funded by the german Federal Ministry of Education and Research (BMBF project 03F0462C). We thank L. Cotrim da Cunha, B. Heinold and I. Tegen, I. Hense, and J. Wu for kindly providing data, and H. Burchard and K. Bolding for technical support.

References

Amon, R. and Benner, R.: Rapid cycling of high-molecular-weight dissolved organic matter in the ocean, Nature, 369, 549–552, 1994. 4319

Armstrong, R., Lee, C., Hedges, J., Honjo, S., and Wakeham, S.: A new, mechanistic model for organic carbon fluxes in the ocean based on the quantitative association of POC with ballast minerals, Deep-Sea Res. Pt. II, 49, 219–236, 2002. 4321

Asper, V. and Smith, W. J.: Abundance, distribution and sinking rates of aggregates in the Ross Sea, Antarctica, Deep-Sea Res. Pt. I, 50, 131–150, doi:10.1016/S0967-0637(02)00146-2, 2003. 4322

Asper, V., Deuser, W., Knauer, G., and Lohrenz, S.: Rapid coupling of sinking particle fluxes between surface and deep ocean waters, Nature, 357, 670–672, 1992. 4322

Aumont, O., Maier-Reimer, E., Blain, S., and Monfray, P.: An ecosystem model of the global ocean including Fe, Si, P colimitations, Global Biogeochem. Cy., 17, 1060, doi:10.1029/2001GB001745, 2003. 4307

Bacon, M. P. and Anderson, R. F.: Distribution of thorium isotopes between dissolved and particulate forms in the deep sea, J. Geophys. Res., 87(C3), 2045–2056, available at: http://dx.doi.org/10.1029/JC087iC03p02045, 1982. 4324

Baker, A., Jickells, T., Biswas, K., Weston, K., and French, M.: Nutrients in atmospheric aerosol particles along the Atlantic Meridional Transect, Deep-Sea Res. Pt. II, 53, 1706–1719, doi:10.1016/j.dsr2.2006.05.012, 2006a. 4311

Baker, A., Jickells, T., Witt, M., and Linge, K.: Trends in the solubility of iron, aluminium, manganese and phosphorus in aerosol collected over the Atlantic Ocean, Mar. Chem., 98, 43–58, 2006b. 4311

Balistieri, L., Brewer, P., and Murray, J.: Scavenging residence times of trace metals and surface chemistry of sinking particles in the deep ocean, Deep-Sea Res., 28A, 101–121, 1981. 4307, 4322, 4324

Barbeau, K., Rue, E., Bruland, K., and Butler, A.: Photochemical cycling of iron in the surface ocean mediated by microbial iron(III)-binding ligands, Nature, 413, 409–413, 2001. 4317, 4318

Barbeau, K., Rue, E., Trick, C., Bruland, K., and Butler, A.: Photochemical reactivity of siderophores produced by marine heterotrophic bacteria and cyanobacteria based on characteristic Fe(III) binding groups, Limnol. Oceanogr., 48, 1069–1078, 2003. 4318

Behrenfeld, M. and Falkowski, P.: Photosynthetic rates derived from satellite-based chlorophyll concentration, Limnol. Oceanogr., 42, 1–20, 1997. 4313

Bergquist, B., Wu, J., and Boyle, E.: Variability in oceanic dissolved iron is dominated by the colloidal fraction, Geochim. Cosmochim. Ac., 71, 2960–2974, doi:10.1016/j.gca.2007.03.013, 2007. 4325, 4326

Bowie, A. R., Maldonado, M. T., Frew, R. D., Croot, P. L., Achterberg, E. P., Mantoura, R. F. C., Worsfold, P. J., Law, C. S., and Boyd, P. W.: The fate of added iron during a mesoscale fertilisation experiment in the Southern Ocean, Deep-Sea Res. Pt. II, 48, 2703–2743, 2001. 4318

Boyd, P. W. and Abraham, E. R.: Iron-mediated changes in phytoplankton photosynthetic competence during SOIREE, Deep-Sea Res. Pt. II, 48, 2529–2550, 2001. 4306

Boye, M., Van den Berg, C., De Jong, J., Leach, H., Croot, P., and De Baar, H.: Organic complexation of iron in the Southern Ocean, Deep-Sea Res. Pt. I 48, 1477–1497, 2001. 4310, 4317, 4318

Boye, M., Aldrich, A., van den Berg, C., de Jong, J., Nirmaier, H., Veldhuis, M., Timmermans,

K., and de Baar, H.: The chemical speciation of iron in the north-east Atlantic Ocean, Deep-Sea Res. Pt. I, 53, 667–683, 2006. 4310, 4315, 4317
Broecker, W. S. and Peng, T.-H.: Tracers in the sea, in: Tracers in the sea, Eldigio Press Lamont Doherty Geological Observatory, 2–5, 1982. 4314
Burd, A. and Jackson, G.: Particle Aggregation, Annual Review of Marine Science, 1, 65–90, doi:10.1146/annurev.marine.010908.163904, 2009. 4322
Coale, K., Johnson, K., Fitzwater, S., Gordon, R., Tanner, S., Chavez, F., Ferioli, L., Sakamoto, C., Rogers, P., Millero, F., Steinberg, P., Nightingale, P., Cooper, D., Cochlan, W., Landry, M., Constantinou, J., Rollwagen, G., Trasvina, A., and Kudela, R.: A massive phytoplankton bloom induced by an ecosystem-scale iron fertilization experiment in the equatorial Pacific Ocean, Nature, 383, 495–501, 1996. 4306
Coale, K. H., Johnson, K. S., Chavez, F. P., Buesseler, K. O., Barber, R. T., Brzezinski, M. A., Cochlan, W. P., Millero, F. J., Falkowski, P. G., Bauer, J. E., Wanninkhof, R. H., Kudela, R. M., Altabet, M. A., Hales, B. E., Takahashi, T., Landry, M. R., Bidigare, R. R., Wang, X., Chase, Z., Strutton, P. G., Friederich, G. E., Gorbunov, M. Y., Lance, V. P., Hilting, A. K., Hiscock, M. R., Demarest, M., Hiscock, W. T., Sullivan, K. F., Tanner, S. J., Gordon, R. M., Hunter, C. N., Elrod, V. A., Fitzwater, S. E., Jones, J. L., Tozzi, S., Koblizek, M., Roberts, A. E., Herndon, J., Brewster, J., Ladizinsky, N., Smith, G., Cooper, D., Timothy, D., Brown, S. L., Selph, K. E., Sheridan, C. C., Twining, B. S., and Johnson, Z. I.: Southern Ocean Iron Enrichment Experiment: Carbon cycling in high- and low-Si waters, Science, 304, 408–414, available at: http://www.sciencemag.org/cgi/content/abstract/304/5669/408, 2004. 4306
Cullen, J., Bergquist, B., and Moffett, J.: Thermodynamic characterization of the partitioning of iron between soluble and colloidal species in the Atlantic Ocean, Mar. Chem., 98, 295–303, 2006. 4310, 4325, 4326
De Boyer Montegut, C., Madec, G., Fischer, A., Lazar, A., and Iudicone, D.: Mixed layer depth over the global ocean: An examination of profile data and a profile-based climatology, J. Geophys. Res.-Oceans, 109, C12003, doi:10.1029/2004JC002378, 2004. 4312, 4346
De La Rocha, C. and Passow, U.: Factors influencing the sinking of POC and the efficiency of the biological carbon pump, Deep-Sea Res. Pt. II, 54, 639–658, doi:10.1016/j.dsr2.2007.01.004, 2007. 4313, 4321
Duce, R. and Tindale, N.: Atmospheric transport of iron and its deposition in the ocean, Limnol. Oceanogr., 36, 1715–1726, 1991. 4311
Falkowski, P.: Evolution of the nitrogen cycle and its influence on the biological sequestration

of CO_2 in the ocean, Nature, 387, 272–275, 1997. 4307
Fischer, G., Ratmeyer, V., and Wefer, G.: Organic carbon fluxes in the Atlantic and the Southern Ocean: relationship to primary production compiled from satellite radiometer data, Deep-Sea Res. Pt. II, 47, 1961–1997, doi:10.1016/S0967-0645(00)00013-8, 2000. 4314
Francois, R., Honjo, S., Krishfield, R., and Manganini, S.: Factors controlling the flux of organic carbon to the bathypelagic zone of the ocean, Global Biogeochem. Cy., 16, 1087, doi:10.1029/2001GB001722, 2002. 4321
Gerringa, L., Veldhuis, M., Timmermans, K., Sarthou, G., and de Baar, H.: Co-variance of dissolved Fe-binding ligands with phytoplankton characteristics in the Canary Basin, Mar. Chem., 102, 276–290, 2006. 4310, 4317, 4318
Gerringa, L., Blain, S., Laan, P., Sarthou, G., Veldhuis, M., Brussaard, C., Viollier, E., and Timmermans, K.: Fe-binding dissolved organic ligands near the Kerguelen Archipelago in the Southern Ocean (Indian sector), Deep-Sea Res. Pt. II, 55, 606–621, 2008. 4310, 4317
Gledhill, M. and van den Berg, C.: Determination of complexation of iron(III) with natural organic complexing ligands in seawater using cathodic stripping voltammetry, Mar. Chem., 47, 41–54, 1994. 4317
Granger, J. and Price, N. M.: The importance of siderophores in iron nutrition of heterotrophic marine bacteria, Limnol. Oceanogr., 44, 541–555, 1999. 4317
Gruber, N., Frenzel, H., Doney, S., Marchesiello, P., McWilliams, J., Moisan, J., Oram, J., Plattner, G.-K., and Stolzenbach, K.: Eddy-resolving simulation of plankton ecosystem dynamics in the California Current System, Deep-Sea Res. Pt. I, 53, 1483–1516, doi:10.1016/j.dsr.2006.06.005, 2006. 4322
Guieu, C., Bozec, Y., Blain, S., Ridame, C., Sarthou, G., and Leblond, N.: Impact of high Saharan dust inputs on dissolved iron concentrations in the Mediterranean Sea, Geophys. Res. Lett., 29(19), 1911, doi:10.1029/2001GL014454, 2002. 4322
Hamm, C.: Interactive aggregation and sedimentation of diatoms and clay-sized lithogenic material, Limnol. Oceanogr., 47, 1790–1795, 2002. 4314, 4321
Heinold, B., Helmert, J., Hellmuth, O., Wolke, R., Ansmann, A., Marticorena, B., Laurent, B., and Tegen, I.: Regional modeling of Saharan dust events using LM-MUSCAT: Model description and case studies, J. Geophys. Res., 112, D11204, doi:10.1029/2006JD007443, 2007. 4322
Honjo, S., Manganini, S., and Poppe, L.: Sedimentation of lithogenic particles in the deep ocean, Mar. Geol., 50, 199–220, 1982. 4321, 4322

Hutchins, D., Witter, A., Butler, A., and Luther III, G.: Competition among marine phytoplankton for different chelated iron species, Nature, 400, 858–861, 1999. 4307, 4318
Hutchins, D., Hare, C., Weaver, R., Zhang, Y., Firme, G., DiTullio, G., Alm, M., Riseman, S., Maucher, J., Geesey, M., Trick, C., Smith, G., Rue, E., Conn, J., and Bruland, K.: Phytoplankton iron limitation in the Humboldt Current and Peru Upwelling, Limnol. Oceano., 47, 997–1011, 2002. 4307
Jackson, G. and Burd, A.: Aggregation in the marine environment, Environ. Sci. Technol., 32, 2805–2814, 1998. 4322
Jickells, T. D., An, Z. S., Andersen, K. K., Baker, A. R., Bergametti, G., Brooks, N., Cao, J. J., Boyd, P. W., Duce, R. A., Hunter, K. A., Kawahata, H., Kubilay, N., laRoche, J., Liss, P. S., Mahowald, N., Prospero, J. M., Ridgwell, A. J., Tegen, I., and Torres, R.: Global Iron Connections Between Desert Dust, Ocean Biogeochemistry, and Climate, Science, 308, 67–71, available at: http://www.sciencemag.org/cgi/content/abstract/308/5718/67, 2005. 4307
Johansen, A., Siefert, R., and Hoffmann, M.: Chemical composition of aerosols collected over the tropical North Atlantic Ocean, J. Geophys. Res.-Atmos., 105, 15277–15312, 2000. 4311
Johnson, K., Coale, K., Elrod, V., and Tindale, N.: Iron photochemistry in seawater from the equatorial Pacific, Mar. Chem., 46, 319–334, 1994. 4307, 4318
Johnson, K., Gordon, R., and Coale, K.: What controls dissolved iron concentrations in the world ocean?, Mar. Chem., 57, 137–161, 1997. 4314, 4324
Klaas, C. and Archer, D.: Association of sinking organic matter with various types of mineral ballast in the deep sea: Implications for the rain ratio, Global Biogeochem. Cy., 16, 1116, doi:10.1029/2001GB001765, 2002. 4321
Kondo, Y., Takeda, S., Nishioka, J., Obata, H., Furuya, K., Johnson, W. K., and Wong, C. S.: Organic iron (III) complexing ligands during an iron enrichment experiment in the western subarctic North Pacific, Geophys. Res. Lett., 35, L12601, doi:10.1029/2008GL033354, 2008. 4318, 4321
Kriest, I.: Different parameterizations of marine snow in a 1D-model and their influence on representation of marine snow, nitrogen budget and sedimentation, Deep-Sea Res. Pt. I, 49, 2133–2162, doi:10.1016/S0967-0637(02)00127-9, 2002. 4322
Lewis, B., Luther, G. I., Lane, H., and Church, T.: Determination of metal-organic complexation in natural waters by SWASV with pseudopolarograms, Electroanal., 7, 166–177, 1995. 4318
Luther, G. I., Rozan, T., Witter, A., and Lewis, B.: Metal-organic complexation in the marine environment, Geochem. T., 2, 65–74, doi:10.1039/b105736g, 2001. 4318

Lutz, M., Dunbar, R., and Caldeira, K.: Regional variability in the vertical flux of particulate organic carbon in the ocean interior, Global Biogeochem. Cy., 16, 1037, doi: 10.1029/2000GB001383, 2002. 4314

Macrellis, H., Trick, C., Rue, E., Smith, G., and Bruland, K.: Collection and detection of natural iron-binding ligands from seawater, Mar. Chem., 76, 175–187, 2001. 4317, 4318

Mahowald, N., Luo, C., Del Corral, J., and Zender, C.: Interannual variability in atmospheric mineral aerosols from a 22-year model simulation and observational data, J. Geophys. Res.-Atmos., 108, 4352(D12), doi:10.1029/2002JD002821, 2003. 4307, 4310, 4330

Maldonado, M. and Price, N.: Utilization of iron bound to strong organic ligands by plankton communities in the subarctic North Pacific, Deep-Sea Res. Pt. II, 46, 2447–2473, 1999. 4307, 4311, 4318

Maldonado, M. T., Strzepek, R. F., Sander, S., and Boyd, P. W.: Acquisition of iron bound to strong organic complexes, with different Fe binding groups and photochemical reactivities, by plankton communities in Fe-limited subantarctic waters, Global Biogeochem. Cy., 19, GB4S23, doi:10.1029/2005GB002481, 2005. 4318

Martin, J. and Fitzwater, S.: Iron deficiency limits phytoplankton growth in the northeast Pacific subarctic, Nature, 331, 341–343, 1988. 4306

Martin, J., Knauer, G., Karl, D., and Broenkow, W.: VERTEX: Carbon cycling in the Northeast Pacific, Deep-Sea Res., 34, 267–285, 1987. 4313

Martin, J., Gordon, R., and Fitzwater, S.: Iron in Antarctic waters, Nature, 345, 156–158, 1990. 4306

Martin, J., Coale, K., Johnson, K., Fitzwater, S., Gordon, R., Tanner, S., Hunter, C., Elrod, V., Nowicki, J., Coley, T., Barber, R., Lindley, S., Watson, A., Scoy, K. V., Law, C., Liddicoat, M., Ling, R., Stanton, T., Stockel, J., Collins, C., Anderson, A., Bidigare, R., Ondrusek, M., Latasa, M., Millero, F., Lee, K., Yao, W., Zhang, J., Friedrich, G., Sakamoto, C., Chavez, F., Buck, K., Kolber, Z., Greene, R., Falkowski, P., Chisholm, S., Hoge, F., Swift, R., Yungel, J., Turner, S., Nightingale, P., Hatton, A., Liss, P., and Tindale, N.: Testing the iron hypothesis in ecosystems of the equatorial Pacific Ocean, Nature, 371, 123–129, 1994. 4306

Martinez, J. and Haygood, M.: Identification of a natural desferrioxamine siderophore produced by a marine bacterium, Limnol. Oceanogr. suppl., 420–424, 2001. 4317

Martinez, J., Carter-Franklin, J., Mann, E., Martin, J., Haygood, M., and Butler, A.: Structure and membrane affinity of a suite of amphiphilic siderophores produced by a marine bacterium, P. Natl. Acad. Sci. USA, 100, 3754–3759, doi:10.1073/pnas.0637444100, 2003.

4317
Martinez, J. S., Zhang, G. P., Holt, P. D., Jung, H.-T., Carrano, C. J., Haygood, M. G., and Butler, A.: Self-assembling amphiphilic siderophores from marine bacteria, Science, 287, 1245–1247, doi:10.1126/science.287.5456.1245, available at: http://www.sciencemag.org/cgi/content/abstract/287/5456/1245, 2000. 4317, 4319
McCave, I.: Size spectra and aggregation of suspended particles in the deep ocean, Deep-Sea Res., 31, 329–352, 1984. 4322
Mills, M., Ridame, C., Davey, M., La Roche, J., and Geider, R.: Iron and phosphorus co-limit nitrogen fixation in the eastern tropical North Atlantic, Nature, 429, 292–294, 2004. 4307
Moffet, J.: Transformations among different forms of iron in the ocean, in: The Biogeochemistry of Iron in Seawater, edited by: Turner, D. and Hunter, K., SCOR/IUPAC Series, J. Wiley, 1–7, 2001. 4324
Moore, R. and Hunter, K.: Thorium adsorption in the ocean: reversibility and distribution amongst particle sizes, Geochim. Cosmochim. Ac., 49, 2253–2257, 1985. 4325
Nyffeler, U., Li, Y.-H., and Santschi, P.: A kinetic approach to describe trace-element distribution between particles and solution in natural aquatic systems, Geochim. Cosmochim. Ac., 48, 1513–1522, 1984. 4324
Parekh, P., Follows, M., and Boyle, E.: Modelling the global ocean iron cycle, Global Biogeochem. Cy., 18, GB1002, doi:1029/2003GB002061, 2004. 4307, 4325
Passow, U.: Switching perspectives: Do mineral fluxes determine particulate organic carbon fluxes or vice versa?, Geochem. Geophy. Geosy., 5, Q04002, doi:10.1029/2003GC000670, 2004. 4321, 4322
Passow, U. and De la Rocha, C.: Accumulation of mineral ballast on organic aggregates, Global Biogeochem. Cy., 20, GB4S23, doi:10.1029/2005GB002579, 2006. 4314, 4321, 4323
Pomeroy, L. R. and Wiebe, W. J.: Temperature and substrates as interactive limiting factors for marine heterotrophic bacteria, Aquat. Microb. Ecol., 23, 187–204, available at: http://www.int-res.com/abstracts/ame/v23/n2/p187-204/, 2001. 4320
Poorvin, L., Rinta-Kanto, J., Hutchins, D., and Wilhelm, S.: Viral release of iron and its bioavailability to marine plankton, Limnol. Oceanogr., 49, 1734–1741, 2004. 4318
Powell, R. and Wilson-Finelli, A.: Photochemical degradation of organic iron complexing ligands in seawater, Aquat. Sci., 65, 367–374, 2003. 4318
Reid, R., Live, D., Faulkner, D., and Butler, A.: A siderophore from a marine bacterium with an exceptional ferric ion affinity constant, Nature., 366, 455–458, 1993. 4317

Reinthaler, T., Van Aken, H., Veth, C., Aristegui, J., Robinson, C., Williams, P. J. B., Lebaron, P., and Herndl, G. J.: Prokaryotic respiration and production in the meso- and bathypelagic realm of the eastern and western North Atlantic basin, Limnol. Oceanogr., 51, 1262–1273, 2006. 4320

Rijkenberg, M., Gerringa, L., Carolus, V., Velzeboer, I., and de Baar, H.: Enhancement and inhibition of iron photoreduction by individual ligands in open ocean seawater, Geochim. Cosmochim. Ac., 70, 2790–2805, 2006. 4318

Rijkenberg, M., Powell, C., Dall'Osto, M., Nielsdottir, M., Patey, M., Hill, P., Baker, A., Jickells, T., Harrison, R., and Achterberg, E.: Changes in iron speciation following a Saharan dust event in the tropical North Atlantic Ocean, Mar. Chem., 110, 56–67, doi:10.1016/j.marchem.2008.02.006, 2008. 4315, 4318

Rose, A. and Waite, T.: Predicting iron speciation in coastal waters from the kinetics of sunlight-mediated iron redox cycling, Aquat. Sci., 65, 375–383, 2003a. 4307, 4316

Rose, A. and Waite, T.: Kinetics of hydrolysis and precipitation of ferric iron in seawater, Environ. Sci. Technol., 37, 3897–3903, 2003b. 4309

Rose, A. and Waite, T.: Kinetics of iron complexation by dissolved natural organic matter in coastal waters, Mar. Chem., 84, 85–103, 2003c. 4319

Rue, E. and Bruland, K.: Complexation of iron(III) by natural organic ligands in the Central North Pacific as determined by a new competitive ligand equilibration/adsorptive cathodic stripping voltammetric method, Mar. Chem., 50, 117–138, 1995. 4310, 4311, 4317, 4318, 4319

Rue, E. and Bruland, K.: The role of organic complexation on ambient iron chemistry in the equatorial Pacific Ocean and the response of a mesoscale iron addition experiment, Limnol. Oceanogr., 42, 901–910, 1997. 4317, 4318

Sarthou, G., Baker, A., Blain, S., Achterberg, E., Boye, M., Bowie, A., Croot, P., Laan, P., De Baar, H., Jickells, T., and Worsfold, P.: Atmospheric iron deposition and sea-surface dissolved iron concentrations in the eastern Atlantic Ocean, Deep-Sea Res. Pt. I, 50, 1339–1352, 2003. 4315

Sarthou, G., Baker, A. R., Kramer, J., Laan, P., Laës, A., Ussher, S., Achterberg, E. P., de Baar, H. J., Timmermans, K. R., and Blain, S.: Influence of atmospheric inputs on the iron distribution in the subtropical North-East Atlantic Ocean, Mar. Chem., 104, 186–202, doi:10.1016/j.marchem.2006.11.004, 2007. 4315

Sato, M., Takeda, S., and Furuya, K.: Iron regeneration and organic iron(III)-binding ligand

production during in situ zooplankton grazing experiment, Mar. Chem., 106, 471–488, doi: 10.1016/j.marchem.2007.05.001, 2007. 4318
Schartau, M. and Oschlies, A.: Simultaneous data-based optimization of a 1D-ecosystem model at three locations in the North Atlantic: Part I. Method and parameter estimates, J. Mar. Res., 61, 765–793, 2003a. 4311
Schartau, M. and Oschlies, A.: Simultaneous data-based optimization of a 1D-ecosystem model at three locations in the North Atlantic: Part II. Standing stocks and nitrogen fluxes, J. Mar. Res., 61, 795–821, 2003b. 4311
Smayda, T.: The suspension and sinking of phytoplankton in the sea (RV), Oceanogr. Mar. Biol., 8, 353–414, 1970. 4322
Spokes, L. and Jickells, T.: Factors controlling the solubility of aerosol trace metals in the atmosphere and on mixing into seawater, Aquat. Geochem., 1, 355–374, 1996. 4311
Steigenberger, S. and Croot, P.: Identifying the processes controlling the distribution of H_2O_2 in surface waters along a meridional transect in the eastern Atlantic, Geophys. Res. Lett., 35, L03616, doi:10.1029/2007GL032555, 2008. 4317
Tovar-Sanchez, A., Sañudo-Wilhelmy, S. A., Garcia-Vargas, M., Weaver, R. S., Popels, L. C., and Hutchins, D. A.: A trace metal clean reagent to remove surface-bound iron from marine phytoplankton, Mar. Chem., 82, 91–99, doi:10.1016/S0304-4203(03)00054-9, 2003. 4307
Trick, C.: Hydroxamate-siderophore production and utilization by marine eubacteria, Curr. Microbiol., 18, 375–378, 1989. 4317
Umlauf, L. and Burchard, H.: Second-order turbulence closure models for geophysical boundary layers. A review of recent work, Cont. Shelf Res., 25, 795–827, 2005. 4308
Van den Berg, C.: Evidence for organic complexation of iron in seawater, Mar. Chem., 50, 139–157, 1995. 4310, 4317
Van Der Loeff, M. R., Helmers, E., and Kattner, G.: Continuous transects of cadmium, copper, and aluminium in surface waters of the Atlantic Ocean, 50° N to 50° S: correspondence and contrast with nutrient-like behaviour, Geochim. Cosmochim. Ac., 61, 47–61, 1997. 4316
Wang, W.-X. and Dei, R.: Biological uptake and assimilation of iron by marine plankton: Influences of macronutrients, Mar. Chem., 74, 213–226, 2001. 4318
Weber, L., Völker, C., Schartau, M., and Wolf-Gladrow, D.: Modeling the speciation and biogeochemistry of iron at the Bermuda Atlantic Time-series Study site, Global Biogeochem. Cy., 19, GB1019, doi:10.1029/2004GB002340, 2005. 4307, 4309, 4316
Weber, L., Völker, C., Oschlies, A., and Burchard, H.: Iron profiles and speciation of the up-

per water column at the Bermuda Atlantic Time-series Study site: a model based sensitivity study, Biogeosciences, 4, 689–706, 2007, http://www.biogeosciences.net/4/689/2007/. 4307, 4308, 4309, 4310, 4311, 4325, 4326, 4330

Wedepohl, K. H.: The composition of the continental crust, Geochim. Cosmochim. Ac., 59, 1217–1232, doi:10.1016/0016-7037(95)00038-2, 1995. 4311

Wells, M. and Goldberg, E.: Colloid aggregation in seawater, Mar. Chem., 41, 353–358, 1993. 4307, 4324

Wen, L.-S., Santschi, P., and Tang, D.: Interactions between radioactively labeled colloids and natural particles: Evidence for colloidal pumping, Geochim. Cosmochim. Ac., 61, 2867–2878, 1997. 4307, 4322, 4324

Wilhelm, S. and Trick, C.: Iron-limited growth of cyanobacteria: Multiple siderophore production is a common response, Limnol. Oceanogr., 39, 1979–1984, 1994. 4317

Wilhelm, S., Maxwell, D., and Trick, C.: Growth, iron requirements, and siderophore production in iron-limited *Synechococcus* PCC 7002, Limnol. Oceanogr., 41, 89–97, 1996. 4317

Witter, A. and Luther III, G.: Variation in Fe-organic complexation with depth in the northwestern Atlantic Ocean as determined using a kinetic approach, Mar. Chem., 62, 241–258, 1998. 4310, 4317

Witter, A., Lewis, B., and Luther, G. I.: Iron speciation in the Arabian Sea, Deep-Sea Res. Pt. II, 47, 1517–1539, doi:10.1016/S0967-0645(99)00152-6, 2000. 4310, 4318

Wu, J. and Boyle, E.: Iron in the Sargasso Sea: Implications for the processes controlling dissolved Fe distribution in the ocean, Global Biogeochem. Cy., 16, 1086, doi:10.1029/2001GB001453, 2002. 4315

Wu, J. and Luther III, G.: Complexation of Fe(III) by natural organic ligands in the Northwest Atlantic Ocean by a competitive ligand equilibration method and a kinetic approach, Mar. Chem., 50, 159–177, 1995. 4317

Wu, J., Boyle, E., Sunda, W., and Wen, L.-S.: Soluble and colloidal iron in the oligotrophic North Atlantic and North Pacific, Science, 293, 847–849, 2001. 4325, 4326

Table 1. Relative importance of different coagulation mechanisms.

Particle size	Settling velocity	Brownian motion	Turbulent shear	Differential settling
10 & 10 μm	5 m d^{-1}	1.14×10^{-18}	1.07×10^{-13}	0
10 & 100 μm	5 & 50 m d^{-1}	3.44×10^{-18}	1.78×10^{-11}	1.98×10^{-11}

Table 2. Parameters in the biological model.

Parameters	Symbol	Unit	Value
maximum growth rate of phytoplankton	μ_{max}	d^{-1}	0.27
phytoplankton mortality	γ_p	d^{-1}	0.04
initial slope P-I curve	α	$m^2\,W^{-1}\,d^{-1}$	0.256
nitrate half-saturation constant	K_N	$\mu mol\,L^{-1}$	0.7
iron half-saturation constant	K_{Fe}	$nmol\,L^{-1}$	0.2
phytoplankton aggregation rate	γ_{p^2}	$(\mu mol\,L^{-1})^{-1}\,d^{-1}$	0.025
maximum grazing rate	g_{max}	d^{-1}	1.575
prey capture rate	ϵ	$(\mu mol\,L^{-1})^{-1}\,d^{-1}$	1.6
assimilation efficiency	γ_{za}	–	0.925
excretion	γ_{zb}	d^{-1}	0.01
quadratic mortality of zooplankton	γ_{z^2}	$(\mu mol\,L^{-1})^{-1}\,d^{-1}$	0.34
detritus remineralisation	γ_d	d^{-1}	0.048
sinking velocity of small particles	w_s	$m\,d^{-1}$	5
sinking velocity of aggregates	w_l	$m\,d^{-1}$	50
coeff. for temp. func. (phytoplankton)	C_{ref}	–	1.066
coeff. for temp. func. (remineralisation)	C_2	–	1.12
PAR:short-wave irradiance ratio	f_{PAR}	–	0.43
attenuation due to chlorophyll	κ	$(mg\,Chl)^{-1}\,L\,m^{-1}$	0.04
maximum Fe:N ratio in organic matter	$Q^{max}_{Fe:N}$	$nmol\,L^{-1}\,(\mu mol\,L^{-1})^{-1}$	0.033
minimum Fe:N ratio in organic matter	$Q^{min}_{Fe:N}$	$nmol\,L^{-1}\,(\mu mol\,L^{-1})^{-1}$	0.0066
mass:N ratio in organic matter	$r_{m:N}$	$g\,mol^{-1}$	159
ligand production rate by phytoplankton	γ_{lp}	$nmol\,L^{-1}\,(\mu mol\,L^{-1})^{-1}\,d^{-1}$	0.5
ligand releasing rate from detritus	γ_{ld}	$nmol\,L^{-1}\,(\mu mol\,L^{-1})^{-1}\,d^{-1}$	0.9
ligand remineralisation	γ_l	d^{-1}	0.038
coagulation rate	k_{coag}	$kg^{-1}\,L^{-1}\,d^{-1}$	31446

Table 3. Parameters in the chemical model.

Parameters	Symbol	Unit	Value
Fe(II)' oxidation rate by O_2	k_{ox1}	$(\mu mol\,L^{-1})^{-1}\,d^{-1}$	0.864
oxygen concentration	$[O_2]$	$\mu mol\,L^{-1}$	214
Fe(II)' oxidation rate by O_2^-	k_{ox2}	$(nmol\,L^{-1})^{-1}\,d^{-1}$	864
Fe(II)' oxidation rate by H_2O_2	k_{ox3}	$(nmol\,L^{-1})^{-1}\,d^{-1}$	6.24
maximal irradiance	ir_{max}	$kW\,m^{-2}$	1978
Fe(III)' photoreduction rate at 30 $\mu Em^{-3}\,s^{-1}$	k_{ph3}	d^{-1}	1.32
FeL_{str} photoreduction rate at 30 $\mu Em^{-3}\,s^{-1}$	k_{phls}	d^{-1}	0.38
FeL_{we} photoreduction rate at 30 $\mu Em^{-3}\,s^{-1}$	k_{phlw}	d^{-1}	7.6
Fe_{col} photoreduction rate at 30 $\mu Em^{-3}\,s^{-1}$	k_{ph1}	d^{-1}	1.32
Fe_p photoreduction rate at 30 $\mu Em^{-3}\,s^{-1}$	k_{ph4}	d^{-1}	20.2
Fe(III)' reduction rate by O_2^-	k_{red}	$(nmol\,L^{-1})^{-1}\,d^{-1}$	1.3×10^4
Fe_{col} formation rate	k_{col}	d^{-1}	2.4
Fe_{lig} formation rate	k_{fel}	$(nmol\,L^{-1})^{-1}\,d^{-1}$	172.8
FeL_{str} conditional stability constant	k_{lsd}	$(mol\,L^{-1})^{-1}$	10^{22}
FeL_{we} conditional stability constant	k_{lwd}	$(mol\,L^{-1})^{-1}$	$10^{20.3}$
Fe(III)' scavenging rate	k_{sca}	$kg^{-1}\,L\,d^{-1}$	2500
Fe_{col} aggregation rate	k_{ag}	$kg^{-1}\,L\,d^{-1}$	1.224×10^6
Fe_{col} re dissolution rate	k_{cd}	d^{-1}	0.41
Fe_p re dissolution rate	k_{pd}	d^{-1}	1.5
O_2^- dismutation rate	k_{dm}	$(nmol\,L^{-1})^{-1}\,d^{-1}$	2.64
O_2^- production rate at 30 $\mu Em^{-3}\,s^{-1}$	$S_{O_2^-}$	$(nmol\,L^{-1})^{-1}\,d^{-1}$	1037
H_2O_2 decay rate	k_{dis}	d^{-1}	0.24
solubility of atmospheric iron	k_{sol}	%	1
Total Cu concentration	$[Cu_T]$	$nmol\,L^{-1}$	1
Cu(I) oxidation rate by O_2^-	k_{cuox}	$(nmol\,L^{-1})^{-1}\,d^{-1}$	8.1×10^5
Cu(II) reduction rate by O_2^-	k_{cured}	$(nmol\,L^{-1})^{-1}\,d^{-1}$	182

BGD
6, 4305–4359, 2009

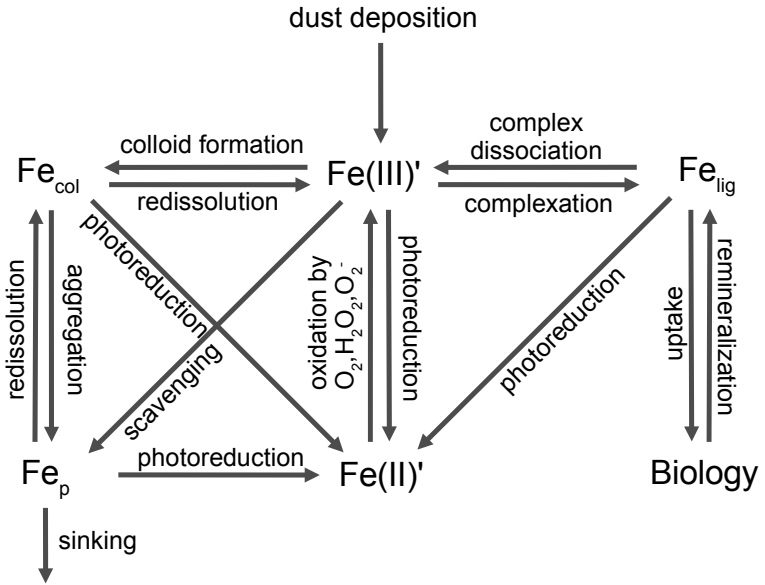

Fig. 1. Schematic representation of processes involved in the cycling of iron in the model.

BGD
6, 4305–4359, 2009

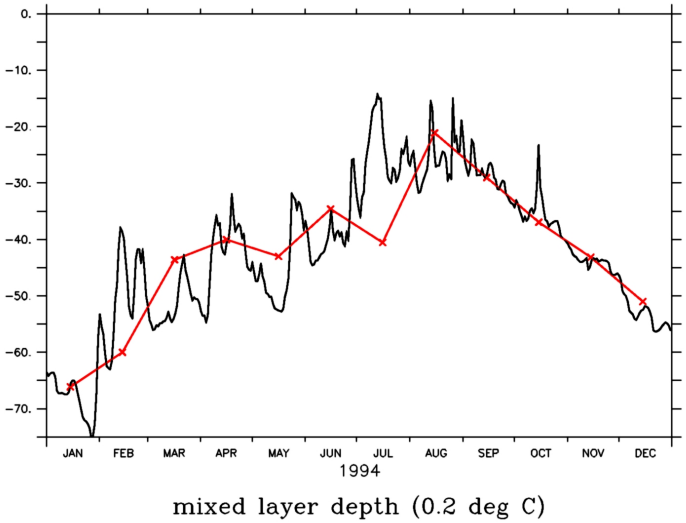

Fig. 2. Comparison of mixed layer depth (m) calculated with a 0.2°C criterium. Black: modelled mixed layer depth, red: climatological estimate by De Boyer Montegut et al. (2004).

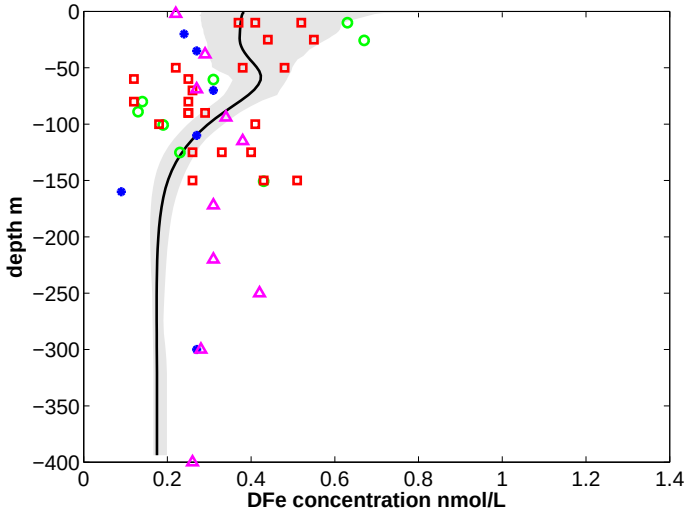

Fig. 3. Modelled DFe concentrations (grey area) compared with measured profiles from Sarthou et al. (2007) (square), data from the cruise POS 332 (triangle), Gerringa et al. (2006) (circle), Rue and Bruland (1995) (star). Modelled mean DFe profile is shown with the black curve.

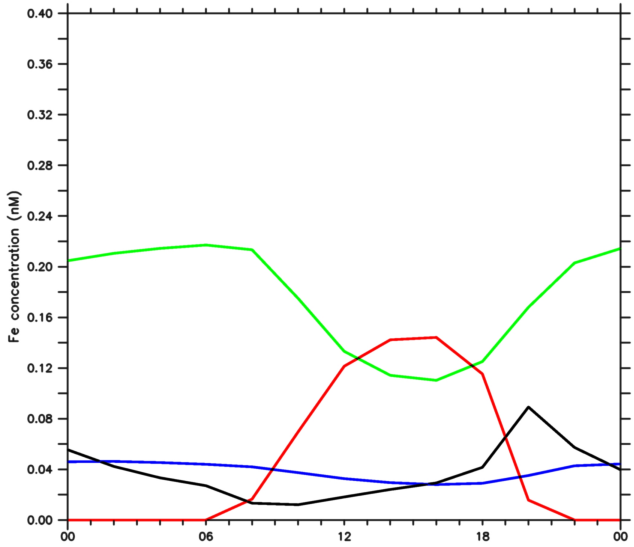

Fig. 4. Modelled diurnal variability of Fe species in summer. Fe(III)': black, Fe(II)': red, Fe_{col}: blue, Fe_{lig}: green.

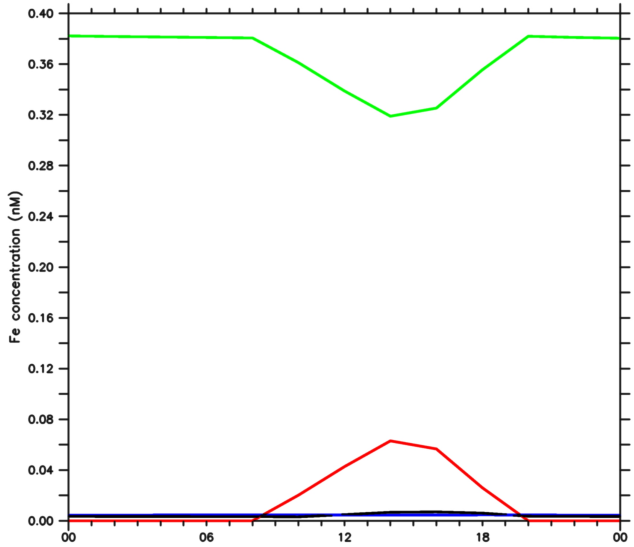

Fig. 5. Modelled diurnal variability of Fe species in winter. Fe(III)': black, Fe(II)': red, Fe_{col}: blue, Fe_{lig}: green.

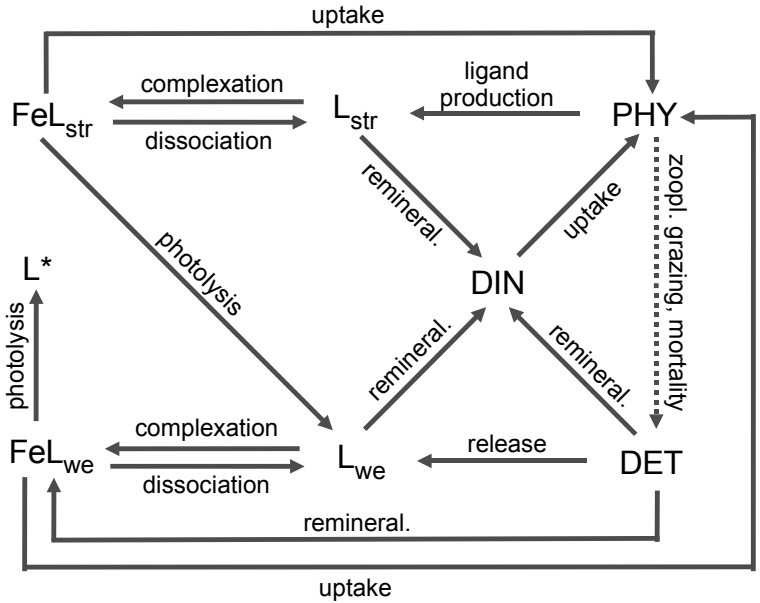

Fig. 6. Schematic representation of sources and fate of organic ligands in the model.

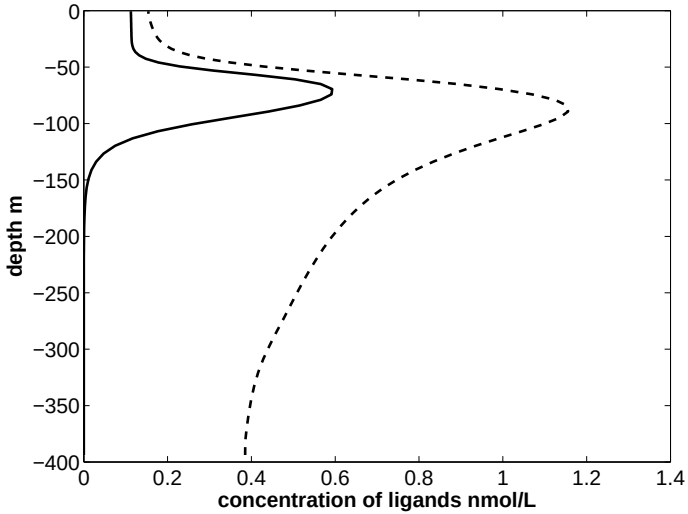

Fig. 7. Modelled annual mean profile of strong (solid) and weak ligands (dashed), nmol L^{-1}.

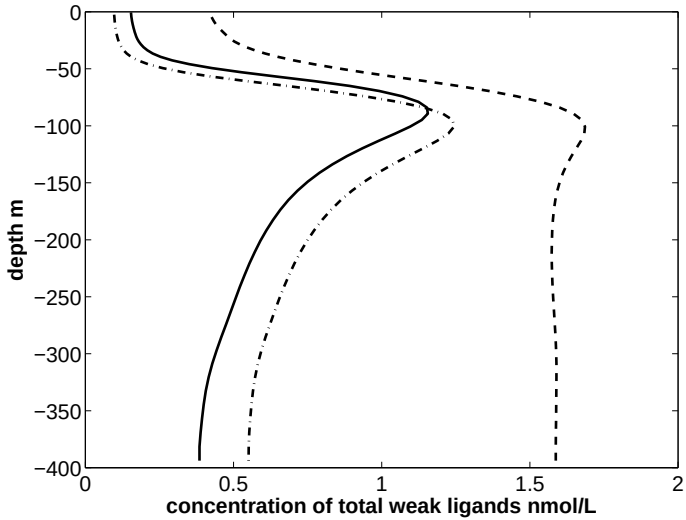

Fig. 8. Annual mean profiles of total weak organic ligands with different Q10 for remineralisation, nmol L^{-1}. Solid line: Q10=2, dash-dot line: Q10=3, dashed line: concentration of total weak ligands restored towards 2 nmol L^{-1}.

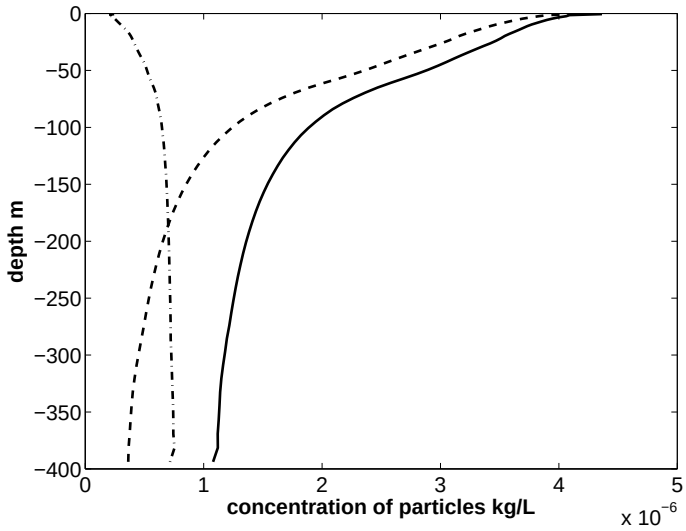

Fig. 9. Annual mean vertical distribution of modelled particles, kg L^{-1}. Solid line: total concentration of particles, dashed line: concentration of small organic and inorganic particles, dash-dot line: concentration of aggregates.

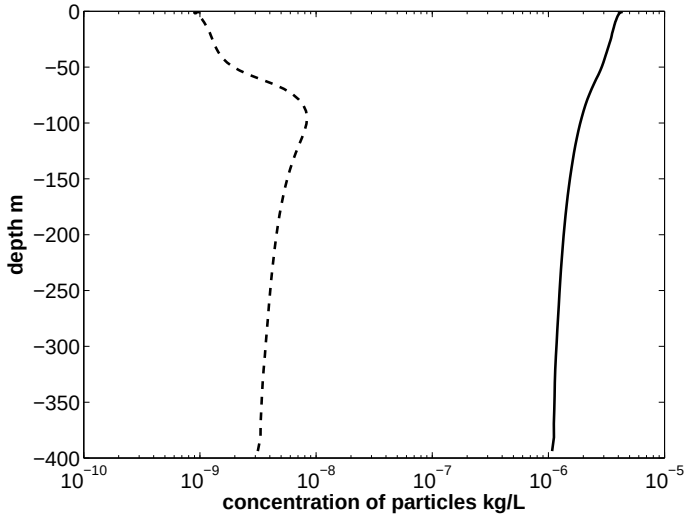

Fig. 10. Comparison of organic and inorganic fraction in particles, $kg\,L^{-1}$. Solid line: dust particles and inorganic fraction in aggregates, dashed line: small organic particles and organic fraction in aggregates.

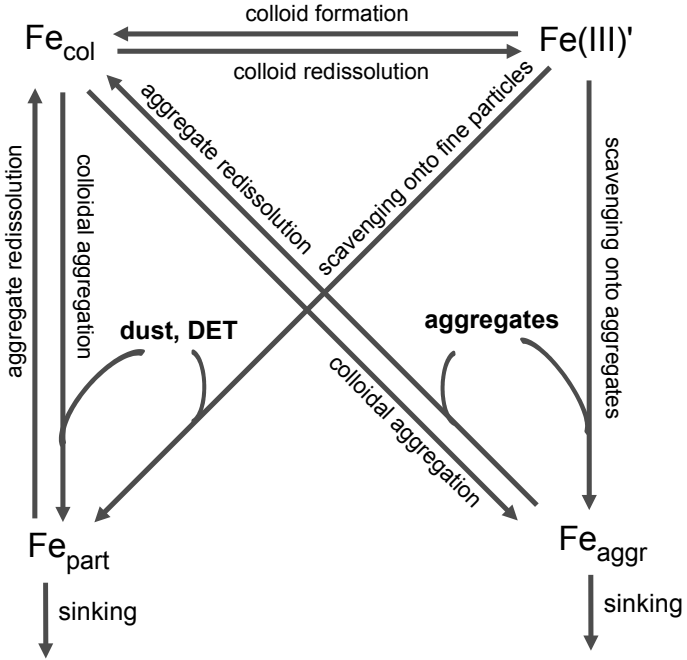

Fig. 11. Schematic representation of DFe removal via scavenging and colloidal aggregation. Fe_{part}: iron bound to surface of small sinking particles, including dust particles and small organic particles (DET), Fe_{aggr}: iron bound to surface of aggregates.

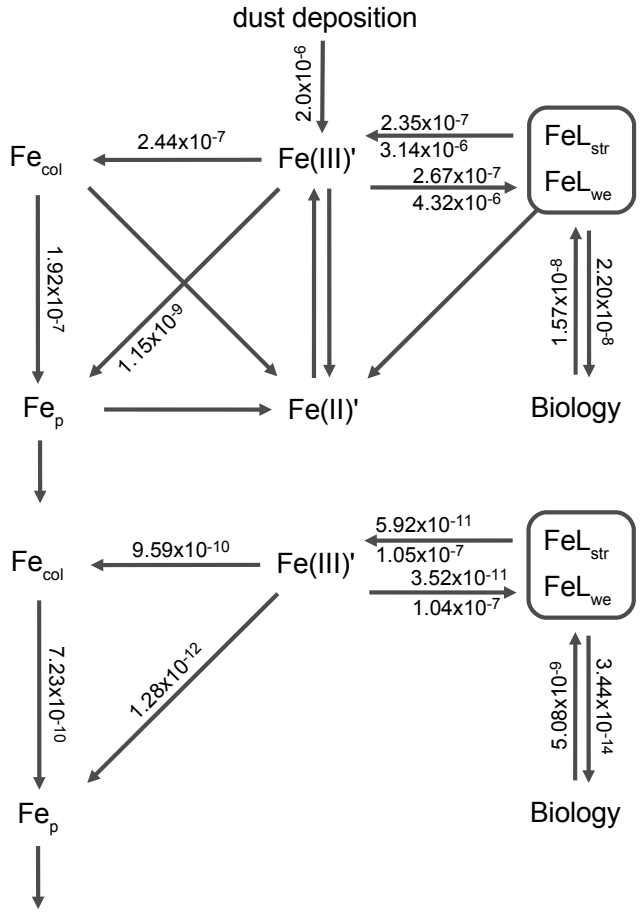

Fig. 12. Fluxes between Fe species in surface and deeper waters, nmol L^{-1} s^{-1}. Upper: integrated for 0–100 m, lower: for 200–300 m.

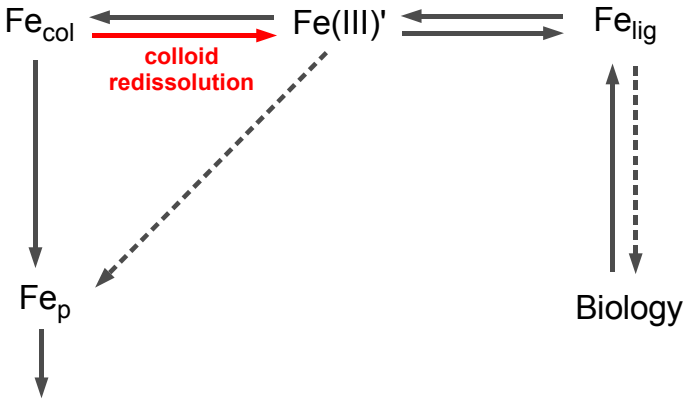

Fig. 13. Processes between Fe species in deeper waters in the first sensitivity study. The additional process is in red and the negligible small fluxes are marked with dashed line.

BGD
6, 4305–4359, 2009

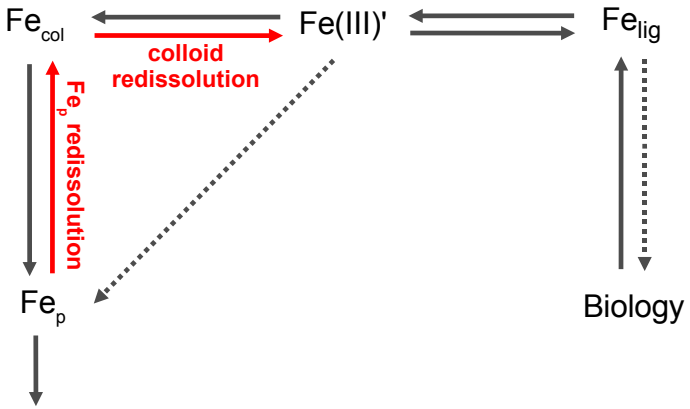

Fig. 14. Processes in deeper waters in the second sensitivity study. The additional process is in red and the negligible small fluxes are marked with dashed line.

BGD
6, 4305–4359, 2009

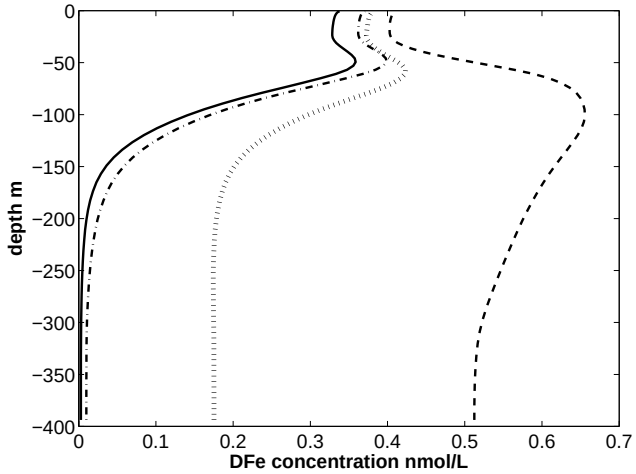

Fig. 15. Modelled annual mean profiles of DFe concentration in the sensitivity studies, nmol L^{-1}. Solid line: without re-dissolution of colloidal or particulate iron; dash-dot line: with re-dissolution of colloidal iron; dashed line: with re-dissolution of colloidal and particulate iron; dotted line: with re-dissolution of colloidal and particulate iron and reduced rate of colloid re-dissolution.